https://doi.org/10.5194/egusphere-2026-4084
Preprint. Discussion started: 22 July 2026

Spatial Downscaling of Pollen-Based Vegetation Reconstructions into Paleo Land Cover Maps

Laura Schild[1], Simeon Lisovski[1], Peter Ewald[1], Julia Walsch[1], Danu Caus[2,3], and Ulrike Herzschuh[1,4,5]

[1]Alfred-Wegener-Institut, Helmholtz-Zentrum für Polar- und Meeresforschung, Research Unit Potsdam, Potsdam, Germany
[2]Helmholtz Centre Hereon, Geesthacht, Germany
[3]Helmholtz AI, Germany
[4]Institute of Biochemistry and Biology, University of Potsdam, Potsdam, Germany
[5]Institute of Environmental Science and Geography, University of Potsdam, Potsdam, Germany

Correspondence: Ulrike Herzschuh (ulrike.herzschuh@awi.de)

Abstract. Past land cover dynamics provide important context for understanding long-term ecosystem responses to climatic change, but paleoecological records are typically sparse, irregular, and site-based. Here, we present a spatial downscaling framework that transforms pollen-derived vegetation reconstructions into gridded paleo land cover maps. The pipeline first translates pollen-based vegetation composition into land cover class frequencies, then distributes these classes within pollen source areas using environmental similarity, and finally applies a U-Net-based interpolation approach to generate spatially continuous reconstructions. We apply the framework to Alaska and western Canada, producing 300 m land cover reconstructions across 15 land cover classes and 119 time slices. The source-area product preserves the direct link to pollen records and contains approximately 2.56 billion reconstructed pixels, while the U-Net-based product extends these reconstructions to continuous spatial coverage across the full study region. Reconstructed land cover trends show broad stability during the late Holocene, with stronger changes around 10 ka BP, including declining evergreen needle-leaved forest cover toward older time slices and corresponding changes in sparse vegetation and shrubland. Relative uncertainty estimates indicate higher uncertainty in forested regions and increasing uncertainty with age, reflecting both class ambiguity and reduced paleo-record support. An example analysis of elevational forest dynamics demonstrates the potential of the dataset for spatially explicit paleoecological applications. The framework provides a bridge between site-based pollen records and landscape-scale analyses, while emphasizing that reconstructed maps represent model-based estimates rather than direct observations of past environments.

1 Introduction

Modern climate change is driving shifts in land cover that create substantial ecological pressures at a global scale (IPBES, 2019; IPCC, 2023). Landscape structures such as habitat connectivity, fragmentation, and the availability of refugia play a pivotal role in species persistence (Fahrig, 2003; Haddad et al., 2015; Zeller et al., 2020). However, predicting local land cover responses remains difficult. While broad-scale patterns of change are relatively well understood, fine-scale responses remain highly uncertain due to the strong spatial heterogeneity of ecosystem dynamics (Franklin et al., 2016; Levin, 1992). Understanding past land cover dynamics may help improve predictions at these smaller spatial scales. Historical observations provide

https://doi.org/10.5194/egusphere-2026-4084
Preprint. Discussion started: 22 July 2026

valuable analogs of long-term vegetation–climate interactions. However, modern observational records are insufficient for this purpose. The instrumental period is too short and encompasses a climatic range that is small relative to the magnitude of projected future climate change (Nieto-Lugilde et al., 2021). The applicability of space-for-time substitutions is further limited by the strong context dependence of ecological processes, which emerge from interactions among climate, edaphic conditions, and disturbance regimes. Consequently, relationships observed across spatial gradients may not remain valid through time. Investigating vegetation dynamics over longer periods, such as throughout the Holocene, can provide the temporal context necessary to capture both long-term climatic variability and vegetation responses across broad environmental gradients (Fordham et al., 2020; Nieto-Lugilde et al., 2021; Seddon et al., 2014).

Among the available paleoecological archives, pollen records provide the broadest spatial coverage and directly encode vegetation composition. Pollen produced by surrounding vegetation is preserved in lacustrine and peat sediments, thereby recording a regional vegetation signal that integrates vegetation across the pollen source area of a site (Faegri and Iversen, 1950). Depending on basin size and depositional context, this source area may extend well beyond 100 km in radius (Githumbi et al., 2021; Schild et al., 2025; Sugita, 2007a). Large numbers of pollen records have been collected and synthesized across broad spatial extents, making pollen one of the most widely available archives for reconstructing past vegetation dynamics (Fyfe et al., 2009; Herzschuh et al., 2022; Vincens et al., 2007; Williams et al., 2018).

Despite these advantages, pollen-based reconstructions also have important limitations. Pollen records are inherently point-based, unevenly distributed in space, and temporally irregular and uncertain (Anderson et al., 2022; Blaauw and Christen, 2011). Furthermore, pollen assemblages represent aggregated regional signals derived from large source areas, resulting in a coarse effective spatial resolution and variable taxonomic resolutions (Bunting et al., 2004; Rull, 2012). These characteristics limit the investigation of fine-scale ecological processes and landscape structure. Habitat configuration, patch arrangement, and local landscape mosaics strongly influence dispersal, connectivity, and ecosystem resilience, yet much of this ecologically relevant heterogeneity is obscured in regional pollen averages. In addition, pollen records only sample a fraction of the landscape and therefore may distort large-scale trends in regions with sparse spatial coverage. Compared to modern satellite-based observations, paleoecological data remain sparse, irregular, uncertain, and indirect. High-resolution reconstructions of past land cover, comparable in structure to modern land cover products, would therefore provide substantial opportunities for investigating ecological dynamics across space and time. Pollen data have been used to reconstruct vegetation dynamics through a range of approaches. Raw pollen compositions can be interpreted directly (Williams et al., 2004), biomes and dominant plant functional types can be reconstructed (Bigelow et al., 2003; Prentice et al., 1996; Tian et al., 2018), and mechanistic models can be applied to correct for taxon-specific biases in pollen productivity and dispersal (Davis, 1963; Sugita, 2007a).

Several approaches have attempted to improve the spatial resolution of pollen-based reconstructions. The Landscape Reconstruction Algorithm (LRA) developed by Sugita (2007a, b) combines the REVEALS model (Regional Estimates of VEgetation Abundance from Large Sites) with the LOVE model (LOcal Vegetation Estimates) to separate regional background signals from local vegetation dynamics. The extended downscaling approach (EDA) by Theuerkauf and Couwenberg (2017) models changes in predefined landscape units through time to reproduce observed pollen assemblages. More recently, BACKLAND (Plancher et al., 2024) reconstructs spatially explicit land cover mosaics by combining LOVE estimates with modern spatial

https://doi.org/10.5194/egusphere-2026-4084
Preprint. Discussion started: 22 July 2026

land cover structure through probabilistic spatial modeling and linear regressions. Other studies have focused on extrapolating pollen-derived vegetation information into regions lacking direct pollen observations. The REVEALS-GMRF (Gaussian Markov Random Field) framework (Pirzamanbein et al., 2018, 2014) combines REVEALS estimates with environmental covariates and spatial statistical models to interpolate vegetation cover continuously across space. Similarly, Zhang et al. (2025) combine spatial and temporal random forest models to generate contiguous maps of past vegetation cover. However, existing reconstructions remain limited in their ability to provide, simultaneously, high spatial resolution, spatial continuity, and temporally continuous representations of land cover dynamics across large regions. Most approaches either preserve the coarse regional character of pollen reconstructions or remain constrained to areas directly surrounding pollen records. As a result, ecologically important information about habitat configuration, patch arrangement, and landscape mosaics remains unresolved.

In this study, we aim to develop a method to create a temporally and spatially continuous high-resolution land cover product for the past 20 ka. We specifically target land cover rather than vegetation composition because land cover products can be integrated directly with modern remote sensing datasets, ecological analyses, and climate modeling frameworks, while also providing interpretable information about habitat structure and landscape connectivity.To achieve this, we developed a spatial downscaling framework consisting of three steps. First, pollen-based vegetation reconstructions are translated into land cover class frequencies. Second, these land cover classes are spatially distributed to pixels within the pollen source area of each record. Third, land cover is interpolated into regions lacking pollen coverage using a convolutional neural network trained on spatial landscape structure. Applying this framework, we produce a temporally and spatially continuous land cover reconstruction for an Alaskan–Canadian study region spanning the last 20 ka. In the following sections, we describe the methodology in detail and evaluate the resulting reconstruction product.

2 Methods

2.1 Downscaling Pipeline

Our pipeline consists of three sequential steps (see Fig. 1). First, pollen-derived vegetation or taxon compositions are converted into land-cover class frequencies using Elastic Net regularized regression. Second, these frequencies are spatially allocated within pollen source areas using the Pixel Flow procedure. Third, the resulting source-area reconstructions are used as spatial training targets for a U-Net model, which interpolates land cover into areas not directly covered by pollen records.

2.1.1 Vegetation cover to land cover

In a first step, pollen-based vegetation information is translated into land cover class frequencies. For this purpose, reconstructed vegetation from the LegacyVegetation dataset is used (Herzschuh et al., 2025; Schild et al., 2025). The dataset provides vegetation estimates reconstructed from sedimentary pollen data based on site- and taxon-specific characteristics, thereby alleviating compositional biases inherent to pollen data (see Fig. 2 for record locations). The spatial resolution differs between sites but is generally regional in scale and corresponds to the estimated pollen source area provided in the LegacyVegetation dataset.

https://doi.org/10.5194/egusphere-2026-4084
Preprint. Discussion started: 22 July 2026

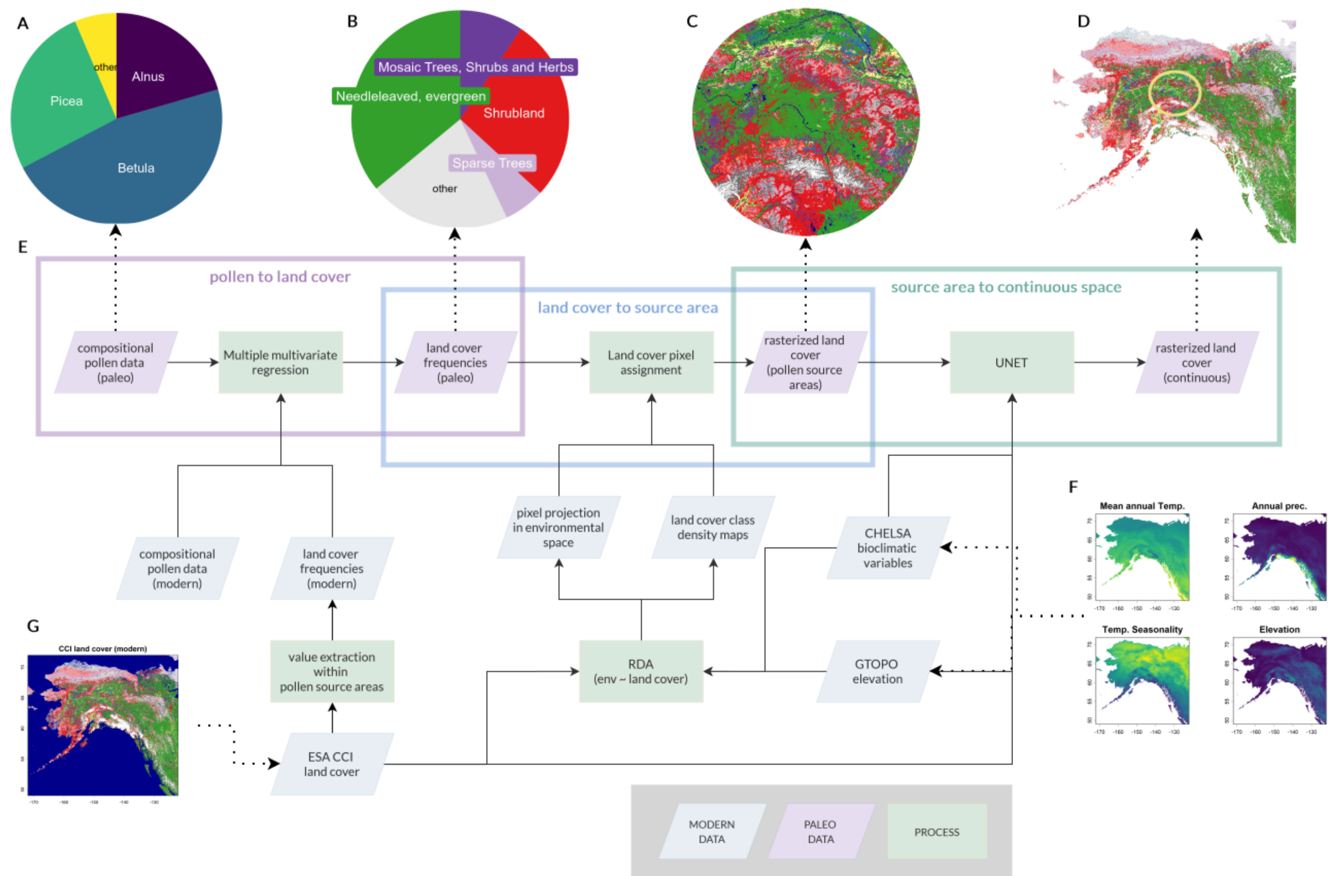

Figure 1. Land cover reconstruction flow chart with illustrated inputs, outputs and intermediate results. The pipeline (e) is separated in three sections: "pollen to land cover", "land cover to source area", and "source area to continuous space". It outlines the evolution of taxonomic pollen compositions (a), to land cover frequencies (b) and spatially explicit land cover maps (c), here illustrated for an example site (see Fig. 1) at 4.5k BP. The fill colors for land cover classes are equivalent to the colors used in (b). Continuous rasterized land cover (d) is the final product after applying a U-Net model. Modern input data at various steps include modern CCI land cover (g) and various modern bioclimatic variables and elevation (f).

https://doi.org/10.5194/egusphere-2026-4084
Preprint. Discussion started: 22 July 2026

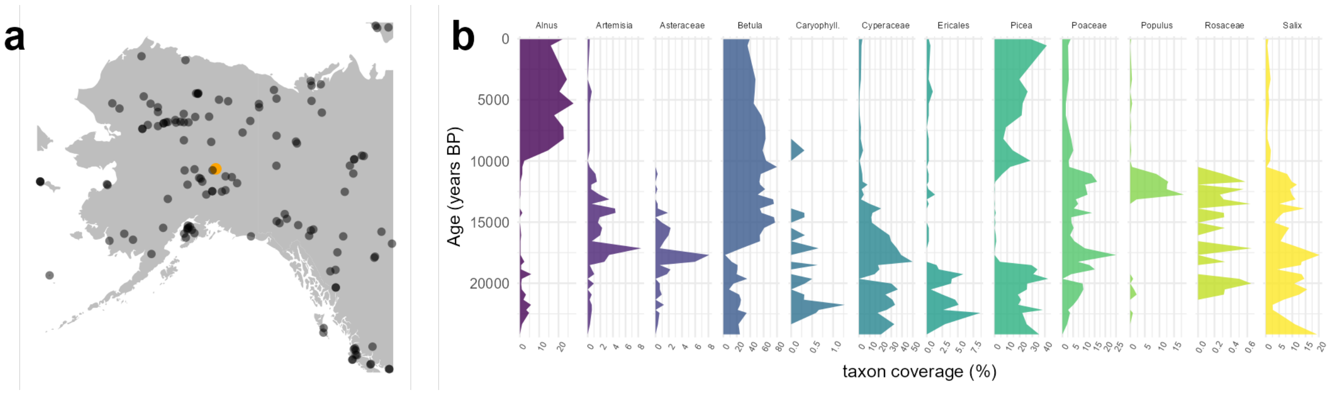

Figure 2. Pollen input data. (a) Map of paleo pollen record locations in Alaska, as available in the LegacyPollen 2.0 data set, with an example record highlighted in orange. (b) Taxonomic composition timeseries throughout the example record.

Temporal resolution and temporal extent are irregular across the dataset. In a first step, this taxonomic and compositional information is translated into land cover frequencies using the relationship between modern land cover and modern pollen samples in a multivariate multiple regression.

The 2020 CCI Land Cover product (300m resolution, ESA, 2017) is used as the modern land cover product. CCI Land Cover is a global multi-satellite product that provides spatially explicit, gridded information on land cover. For each pollen record, the land cover frequencies within the pollen source area were extracted. The original CCI land cover classes were slightly adjusted by merging similar classes, such as all needle-leaf evergreen classes. Anthropogenic classes were excluded because they are not predicted for the past, while the lichen and moss class was kept constant through time (see Appendix A for details).

The regression models are site-specific; that is, a separate model is constructed for each paleo-pollen record to account for regional differences in the relationship between taxonomic composition and land cover classes. Reconstructed vegetation compositions from pollen samples are used as predictor variables, and the corresponding modern land cover frequencies serve as response variables in model construction (see Equation 1). Training data for each regression model are supplemented with additional pollen samples located within the target record's pollen source area and an additional buffer (buffer = 1000km). These additional data consist of modern samples from paleo-pollen records (age < 1 ka BP) and surface pollen samples, which are typically collected for the calibration of climate reconstruction methods (Herzschuh et al., 2023).

To ensure compatibility with compositional data analysis, both predictor and response variables are treated as compositions. Land cover frequencies, provided as percentages, are converted to proportions and renormalized to sum to one. Pollen taxa abundances are likewise normalized to compositions. Zero values in both predictors and responses are handled using a small pseudocount ($\varepsilon = 10^{-6}$) to enable log-ratio transformation. Both predictor and response compositions are then transformed using the centered log-ratio (CLR) transformation prior to model fitting.

$$clr(landcovercomposition) \sim clr(pollencomposition) \quad (1)$$

https://doi.org/10.5194/egusphere-2026-4084
Preprint. Discussion started: 22 July 2026

Model fitting is performed using Elastic Net regularized regression, which combines L1 (lasso) and L2 (ridge) penalties to stabilize coefficient estimates and allow automatic selection of informative taxa (Zou and Hastie, 2005; Aitchison, 1982). This approach is particularly suited to pollen data, where predictors are numerous and often highly correlated. The relative contribution of L1 and L2 penalties is controlled by the mixing parameter α, while the overall strength of regularization is controlled by λ.

The optimal model configuration is determined through cross-validation. Within each outer fold, a grid of α values is evaluated, and for each α the optimal λ is selected using internal cross-validation based on mean squared error in CLR space. Model performance is then assessed on held-out data using the Aitchison distance, which measures differences between compositions in log-ratio space. The final α parameter is chosen as the value that minimizes the mean Aitchison distance across outer folds, and the corresponding λ is re-estimated using the full dataset. To reduce noise from uninformative predictors, taxa with no abundance across the training dataset are excluded prior to model fitting. No further variable selection is imposed, as Elastic Net regularization inherently controls model complexity. Although the final model is constructed using the complete dataset, subsets of the data are used to estimate model performance in a k-fold cross-validation framework (k = 100). If fewer than 100 data points are available, leave-one-out cross-validation is applied. Model performance is evaluated using multiple complementary metrics, including mean absolute error and root mean squared error per class, as well as the Aitchison distance to assess overall compositional accuracy.

Predictions from the regression model are generated in CLR space and subsequently back-transformed to compositions using the inverse CLR transformation (exponentiation followed by renormalization). The resulting compositions are then rescaled to percentages, such that all predicted land cover frequencies are non-negative and sum to 100. The final regression model is then applied to the target paleo-vegetation compositions, which were binned and linearly interpolated to 500-year intervals to remove temporal irregularities.

2.1.2 Land Cover to Source Area - Pixel Flow

To inform the spatial distribution of land cover classes across pixels within the record's pollen source area, the modern environmental space is used. Modern bioclimatic data and land cover classes are extracted from a stratified sample of pixels within the pollen source area and supplemented with pixels from buffer zones surrounding the record, should more data be needed (minimum 50 and maximum 800 pixels per land cover class, see Table 1 for list of environmental variables). The environmental data are z-transformed, and the dataset then used to construct an RDA. This method constrains the environmental variables by land cover class assignments and then performs PCA on the fitted values. The resulting dimensionality reduction maximizes the variation in environmental variables that best explains differences between land cover classes. Anthropogenic classes were excluded from the RDA since their presence is only marginally connected to environmental variables.

Land cover class densities within the RDA space are calculated using a two-dimensional kernel density estimation (kde2d) from the MASS package in R (Venables and Ripley, 2002). This allows calculation of land cover class overlap and distances in this environmental space. Pairwise class distance is calculated as the Hellinger distance (H), which combines pairwise landcover probabilities across the RDA space (see Equation 2).

https://doi.org/10.5194/egusphere-2026-4084
Preprint. Discussion started: 22 July 2026

Table 1. List of environmental variables used for the construction of the reduced-dimensionality environmental space.

Variable	short name	source
Mean Annual Near-Surface Air Temperature	bio01	CHELSA-bioclim 1981-2010 (Brun et al., 2022)
Temperature Seasonality	bio4	
Annual Daily Mean Near-Surface Air Temperature Range	bio7	
Mean Daily Mean Near-Surface Air Temperature of the Warmest Quarter	bio10	
Mean Daily Mean Near-Surface Air Temperature of the Quarter	bio11	
Annual Precipitation	bio12	
Mean Monthly Precipitation of the Warmest Quarter	bio18	
Mean Monthly Precipitation of the Coldest Quarter	bio19	
Growing Degree Days Heat Sum above 0 °C	gdd0	
Growing Degree Days Heat Sum above 5 °C	gdd5	
Growing Degree Days Heat Sum above 10 °C	gdd10	
elevation (asl)	elev	Etopo 2022 (MacFerrin et al., 2025)

$$H = \sqrt{(\sum(\sqrt{p_i} - \sqrt{q_i})^2/\sqrt{2}} \qquad (2)$$

A transport function uses the Hellinger distances as a cost matrix and calculates the least-cost flow of land cover classes between time steps using a fast implementation of the network simplex algorithm (Bonneel et al., 2011; Schuhmacher et al., 2024). This assumes that land cover transitions are more likely to occur between environmentally similar classes and outputs the amount of pixels switching from an original class to a target class. Stronger transitions can also occur in this framework if the reconstructed land cover frequencies require such a change .

The reconstruction proceeds backward in time, starting from the modern land cover map. For each time step, pixels within the pollen source area are projected into the reduced ordination space derived from the RDA model. For the modern time slice, pixels with anthropogenic land cover classes are first reassigned to potential natural vegetation in a preprocessing step. To achieve this, the density maps in RDA space are scaled by the frequencies of land cover classes present within the pollen source area. The natural land cover class for each pixel is then determined as the class whose centroid in ordination space lies closest to the pixel. Euclidean distances between each pixel and the centroids of all land cover classes are then calculated. The class centroids are derived from kernel density estimates of the training data. Pixel transitions between land cover classes, as given by the transport function, are subsequently allocated iteratively. For a given origin class, candidate pixels are evaluated against all permissible target classes and assigned to the closest class in ordination space. Pixels are prioritised by increasing distance to the respective target centroid, and transitions are applied until the required number of pixels for each class transition is reached. The procedure continues until all prescribed transitions for the time step have been completed.

https://doi.org/10.5194/egusphere-2026-4084
Preprint. Discussion started: 22 July 2026

2.1.3 Source area to continuous space (U-Net interpolation)

The previous analysis steps produced spatially explicit land cover maps for the source areas of the available pollen records. To estimate land cover in areas not covered by pollen records, a deep learning method was applied. U-Nets are convolutional neural networks originally developed for image analysis (Ronneberger et al., 2015) and widely applied in land cover classifications due to their spatial coherence (Kramarczyk and Hejmanowska, 2023; Mahmoud et al., 2026). We trained a separate fully convolutional U-Net segmentation network for each paleo time slice to predict land cover class probabilities based on the targets reconstructed from pollen records. The models form a chain in which the prediction for one time slice serves as an additional input channel for the respective next, older time slice, resulting in a processing sequence into the past. Through this time-recurrent structure, the method preserves the temporal coherence of the reconstruction and propagates information from the data-rich, younger end of the chain into the data-poorer, older time slices. Each model is trained individually so that it can capture the relationship between the stationary climatic space and the pollen-based land cover labels. The reconstruction framework was implemented in Python 3.11.15 using PyTorch 2.5.1 and CUDA 12.1. Model training and inference were performed on a high-performance computing node equipped with an NVIDIA A100-SXM4-40GB GPU (40 GB VRAM), two AMD EPYC 7742 64-core processors, and 1 TB of system memory.

Input channels and labels

Each U-Net receives an input tensor with fourteen channels. The first twelve channels contain continuous climate and topography predictors (see Table 1), the thirteenth channel contains the current land cover as a temporally invariant reference or anchor state, and the fourteenth channel contains the predicted land cover of the immediately preceding time slice. For the first time slice in the sequence, which has no predecessor, the fourteenth channel is formed by the modern land cover itself. The twelve climate bands are z-standardized using global averages and standard deviations; these statistics are determined once and reused for all tiles to ensure consistent normalization. Since the two land cover channels carry discrete class information, they are each multiplied by a scaling factor (default value = 0.35) before concatenation with the continuous climate bands so that they do not dominate the normalized climate bands in the input space.

Rather than treating paleo land cover observations as deterministic labels, observer votes were converted into probabilistic soft targets at pixels where pollen-based reconstructions overlap (see Equation 3. Instead of hard single-class labels, soft target distributions are formed to explicitly capture the uncertainty among these observers (Bressan et al., 2022). First, the raw votes are redistributed using an ecological class distance matrix D (see Appendix B). Through a softmax weighting of the form softmax$(-D/\tau)$, votes for a class are proportionally transferred to ecologically similar classes, so that the resulting target distribution reflects the structural similarity between land cover types. Next, a Dirichlet pseudo-count $\alpha 0$ is added to the redistributed votes, and a normalization yields the soft target probabilities (Joo et al., 2020).

$$y_{soft} = \frac{votes + \alpha_0}{\sum_k (votes_k + \alpha_o)} \tag{3}$$

Only pixels with valid observations contribute to the training loss, that is, pixels that lie both within the observation mask and the land mask and for which at least one vote is available.

Composite loss function

https://doi.org/10.5194/egusphere-2026-4084
Preprint. Discussion started: 22 July 2026

The training loss (see Equation 4) is a weighted sum of complementary terms with the standard weights λ = (1.0, 0.3, 1.5, 0.3, 0.1).

$$L = \lambda_1 L_{CE} + \lambda_2 L_{dist} + \lambda_3 L_{focal} + \lambda_4 L_{dice} + \lambda_5 L_{Dirichlet} \tag{4}$$

The first term is a class-weighted soft cross-entropy between the predicted distribution and the soft target. The second term penalizes predictions proportionally to the expected ecological distance between the predicted and target classes; misclassifications between ecologically similar classes are thus penalized less severely than those between dissimilar classes. The focal term modulates the loss by a factor of $(1-p_t)^\gamma$ ($\gamma_{default}$ = 3.0) and directs the optimization toward pixels that are difficult to classify (Lin et al., 2018). The soft-dice term provides a region-based overlap measure that is robust to class imbalance (Milletari et al., 2016; Sudre et al., 2017), and the Dirichlet term forms the negative log-likelihood of a Dirichlet prior, which sharpens and calibrates the prediction distributions. Additionally, a temporal consistency term is added, weighted by $\lambda_{temporal}$ (default value = 0.18), which penalizes unnecessary deviation from the prediction of the previous time slice (see Equation 5).

$$L \mathrel{+}= \lambda_{\text{temporal}} \cdot \text{mean}\left[\mathbb{1}\left(\hat{y} \neq y_{\text{prev}}\right)\right] \tag{5}$$

This term is evaluated exclusively on those pixels where the predecessor provided a valid and sufficiently reliable prediction, i.e., one with a confidence level above a threshold (default value = 0.60). In this way, drift along the chain is dampened without suppressing genuine ecological transitions.

Stabilization of the Chain

Because the amount of available data decreases with increasing age, there is a risk that errors will accumulate along the chain (chain drift). Several mechanisms counteract this effect. Each model is initialized using a warm start with the weights of the preceding chain link rather than randomly, which accelerates and stabilizes training. Through planned teacher forcing, the predecessor channel is blended more heavily with the modern land cover at the start of training (initial value = 0.35) and linearly reduced to a small proportion toward the end of training (final value = 0.08). Confidence gating replaces the predecessor channel in regions with low predecessor confidence (<0.50) with a mixture of the predecessor and modern land cover, thereby limiting the propagation of uncertain predictions. At the same time, the influence of modern land cover for older time slices decreases linearly to a minimum value, since the present-day state becomes increasingly less informative for very old time slices. For older time slices, the learning rate can be gradually reduced, and an ensemble of multiple models trained with different random seeds can be averaged to reduce prediction variance. Finally, time slices with very few valid pixels receive a reduced number of training steps.

Handling class Imbalance

Land cover classes are highly unevenly distributed, a known issue in remote-sensing semantic segmentation. Class imbalance was addressed at both the loss and sampling levels: adaptive class weights were derived from class frequencies, following common inverse-frequency, median-frequency, and logarithmically bounded weighting strategies; rare-class tiles were sampled more frequently; and misclassified rare-class pixels were emphasized through hard negative mining (Badrinarayanan et al.,

https://doi.org/10.5194/egusphere-2026-4084
Preprint. Discussion started: 22 July 2026

2016; Paszke et al., 2016; Shrivastava et al., 2016).

Network architecture and optimization

The architecture consists of a U-Net with fourteen input channels, a class-dependent output dimension, and a base width of 64 channels. Optimization is performed using the AdamW algorithm with a weight regularization of 10-4 and a default learning rate of 3×10^{-3}, optionally with cosine annealing of the learning rate (Loshchilov and Hutter, 2019). Gradients are clipped to a global norm of 1.0. The batch size was set to eight, and for data augmentation, arbitrary rotations by multiples of 90° (i.e. 0°, 90°, 180°, or 270°) were consistently applied to all tensors, including the predecessor channel. By default, 1,500 training steps are performed per time slice as a tradeoff between sufficient model learning and manageable computation time. Tiles were divided into a training set and a validation set.

Tile-Based Training and Inference Due to the size of the grid, training and inference are performed tile by tile. Training was performed on 256 × 256 pixel tiles without overlap, whereas inference used 256 × 256 pixel tiles with 128-pixel overlap. During inference, overlapping tiles (edge length 256 pixels, overlap 128 pixels) are combined using an edge-weighted confidence scheme: For each pixel, the prediction with the highest edge-weighted confidence is adopted, thereby reducing visible tile seams. Ocean pixels are set to a "nodata" value using a sea mask. For each time slice, a class map, a confidence map, and the model checkpoint are output. The amount of training tiles decreases with increasing timeslice age (max = 871, min = 340).

Evaluation metrics

During training, the overall accuracy, the balanced accuracy (defined as the average of the class-wise recall rates), Cohen's κ, and a majority baseline, that is, the proportion of the most frequent class, are continuously logged. These metrics are averaged over the last one hundred steps from an accumulated confusion matrix on the valid pixels. The final balanced accuracy of each time slice is recorded in a log file and serves as a key metric for comparing the time slices along the chain. The accuracy of the final model trained with complete data is also recorded.

2.2 Estimating uncertainty

True validation of both the Source Area reconstruction as well as the U-Net interpolation is not possible because of the lack of independent paleo land cover data. This is especially true at the presented spatial resolution. We therefore estimate uncertainty at each step in the pipeline and generate a relative estimate of uncertainty in the final class assignments.

The performance of the Elastic Net regression (Vegetation to Land Cover, see Section 2.1.1 and Fig. 1) is used to estimate uncertainty in the conversion from pollen to land cover. The uncertainty for each record is calculated from the regression's normalized Aitchison RMSE (NARMSE) value using equations 6 and 7. NARMSE is based on the Aitchison distance between predicted and observed compositions (d_i) at each pollen record location i and normalized using the Aitchison RMSE of the null model, which is defined as the average of all compositions. Lower NARMSE values indicate better model performance.

$$RMSE_A = \sqrt{\frac{1}{n}\sum_{i=1}^{n} d_i^2} \tag{6}$$

https://doi.org/10.5194/egusphere-2026-4084
Preprint. Discussion started: 22 July 2026

$$NARMSE = \frac{RMSE_A}{RMSE_{A,null}} \tag{7}$$

The resulting uncertainty estimates are scaled between 0 and 1 using a robust sigmoid transform following the equations below, where X are the original uncertainty values. The median (m) and the interquartile range (s) are calculated to standardize values to zi (Equation 8). The logistic sigmoid is then applied to yield the final scaled values yi (Equation 9). The transform allows for a final common range of uncertainty values, while reducing the influence of outliers (Fulcher et al., 2013). Overall, this leads to a relative measure of uncertainty within the reconstruction. An absolute uncertainty estimate cannot be made.

$$z_i = \frac{x_i - m}{s} \text{ (where m = median)} \tag{8}$$

$$y_i = \frac{1}{1 - e^{-z_i}} \tag{9}$$

Overlap among land cover classes in RDA space is used as an estimate of uncertainty in the pixel assignment step (Land Cover to Source Area, see Section 2.1.2 and Fig. 1), with less overlap leading to better land cover class distinction and more certain pixel assignment. Overlap was defined as 1 - Hellinger distance between land cover class clusters. The average overlap per site was used as the uncertainty estimate. The resulting values were transformed using the robust sigmoid transform as described above (Equations 8 and 9). Because both regression and pixel assignment uncertainty are only available for the source areas of the pollen records included, we assign weighted means for empty areas at varying spatial resolutions.

In a next step, we estimate the temporal uncertainty by checking the pollen records' reconstructed land cover for consistency. We investigate the agreement in pixel assignments in areas where two or more records overlap. This allows for comparing the consistency with which land cover classes are assigned to specific pixels. To do so, we use two agreement metrics. The first is absolute agreement, where pixels either match or do not match in the assigned land cover. The second is weighted agreement, where ecological similarity between land cover classes is used to compute a distance measure between the two assigned land cover classes. This allows for a more nuanced comparison. The distances between land cover classes were derived from the average land cover class distances in the RDAs of all records in the case study area. RDA details are described in Section 2.1.2 and the distance matrix is included in Appendix B. Temporal uncertainty is spatially explicit for each overlap area and is interpolated for the rest of the study area for each time slice.

Total relative uncertainty is calculated by computing the mean of regression ($UReg$), RDA ($URDA$), temporal ($Utemp$), U-Net training error rate ($UError$), and output U-Net uncertainty ($Uunc$) (see Section 2.1.3) for each pixel i and time slice j.

$$Utotal_{i,j} = \frac{UReg_i + URDA_i + Utemp_{i,j} + UError_j + Uunc_{i,j}}{5} \tag{10}$$

2.3 Application: Analysis of Elevational Tree Cover Dynamics

As an example of how the reconstructed land cover dataset can be used, an analysis of temporal changes in treeline elevation was conducted for a selected pollen record (highlighted in orange in Fig. 2). For each time slice, all pixels classified as

https://doi.org/10.5194/egusphere-2026-4084
Preprint. Discussion started: 22 July 2026

evergreen needle-leaved forest within the source area of the selected record were identified. Based on these pixels, two metrics were computed. First, the proportional forest cover was calculated as the fraction of pixels classified as evergreen needle-leaved forest relative to the total number of pixels within the considered area. Second, elevation values were extracted for these forest pixels from theDEM for these pixels. To approximate the upper elevational limit of forest cover, the 90th percentile of the elevation distribution of evergreen needle-leaved forest pixels was used as a proxy for the treeline. This percentile-based approach reduces sensitivity to isolated high-elevation pixels and provides a robust estimate of the upper forest boundary. Tests with lower percentile thresholds yielded similar temporal trends, indicating that the results are not strongly dependent on the exact percentile choice. All calculations were performed independently for each time slice, allowing the reconstruction of temporal trajectories in both forest cover extent and elevational distribution.

3 Results

3.1 Land cover reconstructions within the pollen source areas

The primary output of the pipeline consists of spatially explicit land cover reconstructions generated within the pollen source areas of individual paleoecological records. Each reconstruction represents a gridded land cover map for a given time slice, where pixels are assigned to one of the predefined land cover classes based on the reconstructed vegetation composition and its position in environmental space. The spatial domain of these source-area-reconstructions is defined by the spatial extent of all pollen source areas included in the study, covering Alaska and large parts of western Canada. Within these areas, land cover is resolved at a spatial resolution of 300 m, allowing for fine-grained representation of local landscape heterogeneity.

Temporarily, the reconstruction spans 119 discrete time slices, covering the full extent of the paleo-records used in this study. These time slices represent interpolated intervals of vegetation composition, providing a continuous temporal framework rather than isolated snapshots. As a consequence of this interpolation, reconstructed land cover reflects temporally smoothed conditions within each slice. The thematic resolution comprises 15 land cover classes (derived from CCI: ESA, 2017) , including both dynamic vegetation types and a subset of static classes that remain constant through time (e.g. water bodies or permanent ice; see Appendix A). In the study area needleleaved evergreen forests, grasslands and shrublands are among the most common land cover classes (see Fig. 3, 4).

Across all time slices, the pipeline produced a total of 2,555,751,577 reconstructed pixels, corresponding to an average of 21,476,904 pixels per time slice. The distribution of reconstructed pixels through time is not uniform and reflects the availability and temporal density of pollen records, as illustrated by the total number of pixels (see Fig. 4). Spatial patterns of reconstructed land cover are shown in Fig. 3. The analysis of spatially aggregated land cover trends is influenced by the temporal availability of pollen records, as the number of contributing source areas varies through time. In particular, earlier time slices are based on fewer records, while the number of available records increases toward the Holocene, affecting the spatial representativeness of aggregated trends.

To account for this, pixel counts of individual land cover classes from 20 ka BP onward are shown in Fig. 4. From approximately 10 ka BP, the number of available records reaches its maximum, providing the most spatially extensive and internally

https://doi.org/10.5194/egusphere-2026-4084
Preprint. Discussion started: 22 July 2026

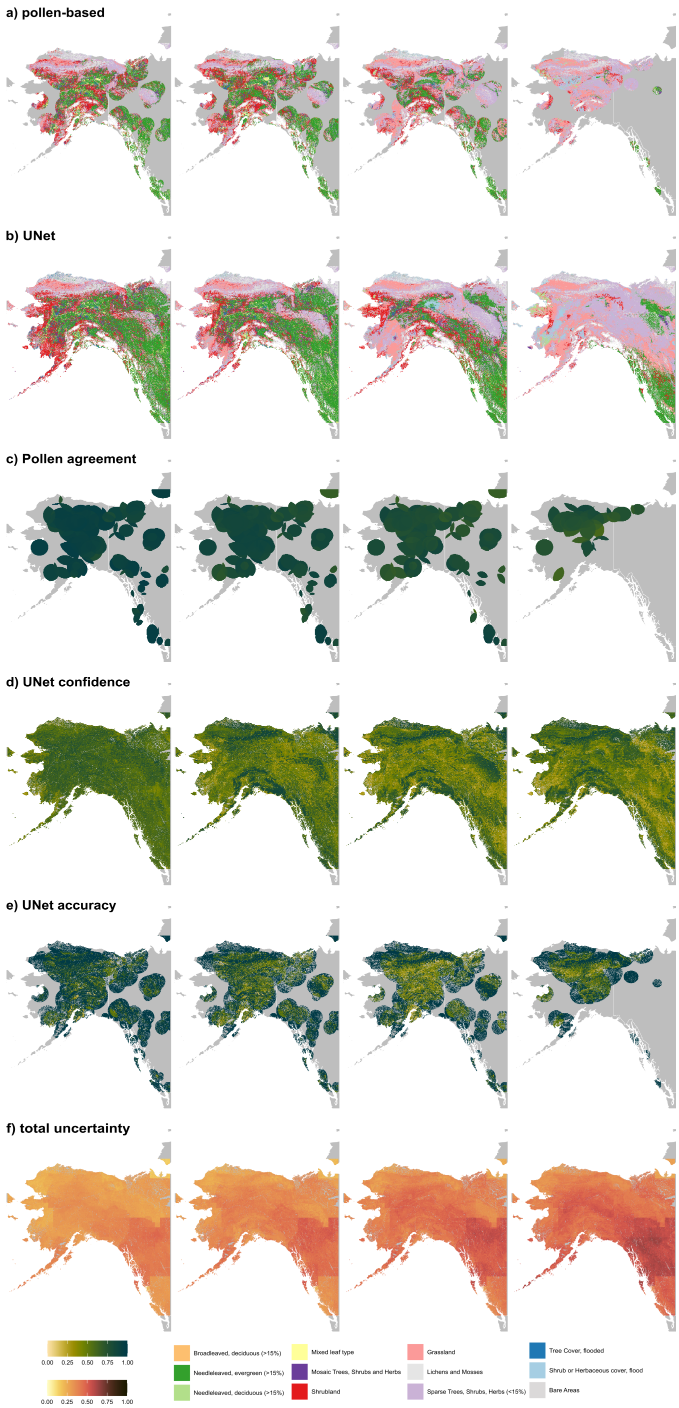

Figure 3. Reconstruction results and performance metrics for example time slices. a) Land cover classes from Source-area reconstruction and b) spatially-continuous reconstruction, c) Land Cover agreement of pollen record overlaps in the source-area reconstruction, d) Internal UNet confidence, e) Validation of full UNet model with labels from the source-area reconstruction, f) relative pipeline uncertainty including uncertainty from source-area reconstruction, U-Net confidence, and temporal trends.

https://doi.org/10.5194/egusphere-2026-4084
Preprint. Discussion started: 22 July 2026

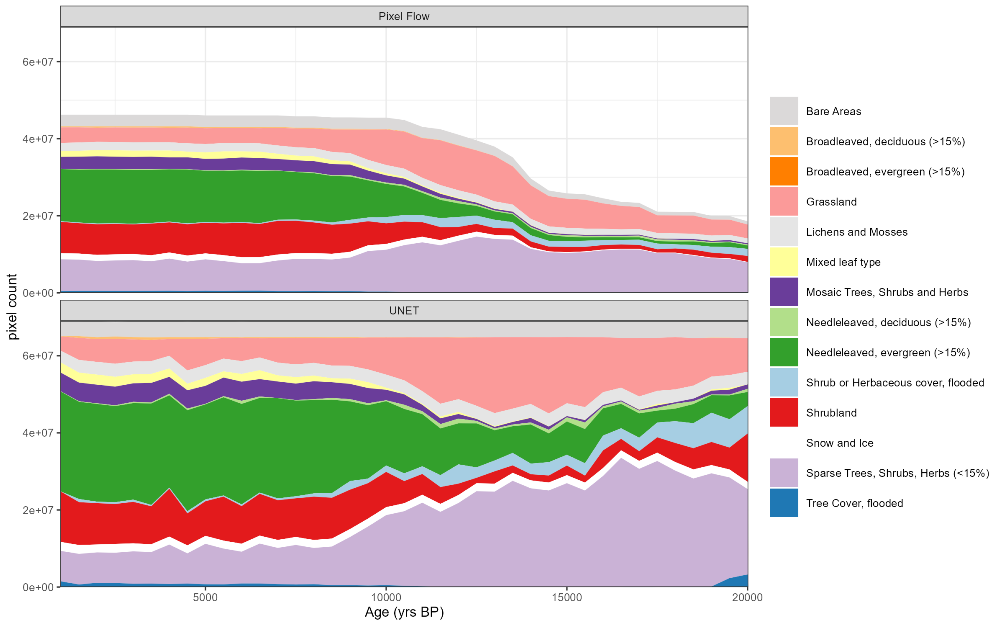

Figure 4. Reconstructed land cover trends for source area reconstruction and spatially continuous reconstruction. The y-axis represents total pixels and highlights the lower spatial coverage with increasing age for the Pixel Flow product (source area reconstruction). General land cover trends are similar between 10ka and present. Between 10ka and 20ka the U-Net predicts largely open landscapes.

consistent reconstruction period. During this interval, land cover composition remains comparatively stable over several millennia. Within this generally stable period, only moderate changes in class proportions are observed. Evergreen needle-leaved tree cover shows a gradual increase through time, while shrubland reaches a maximum extent around 5 ka BP. In contrast, sparse vegetation and grassland classes exhibit a reduction in areal extent over the same period. Overall, the observed temporal trends reflect both underlying vegetation dynamics and the varying spatial coverage of pollen records through time.

3.2 U-Net-based Interpolation of Land Cover Reconstruction

In addition to the source-area reconstructions, a spatially continuous land cover product was generated using a U-Net-based interpolation approach. The resulting output consists of gridded land cover maps for each time slice, where every pixel across the entire study region is assigned to one of the predefined land cover classes. As such, a single output represents a fully continuous paleo land cover reconstruction, in contrast to the spatially discontinuous, record-centered nature of the source-area reconstructions.

The thematic and temporal characteristics of the U-Net-based reconstruction are equivalent to those of the source-area product. Land cover is represented using the same set of 15 classes, and reconstructions are provided for the same 119 time slices, ensuring direct comparability between both datasets.

https://doi.org/10.5194/egusphere-2026-4084
Preprint. Discussion started: 22 July 2026

The key difference lies in spatial extent and structure. While the source-area reconstructions are limited to the spatial influence of individual pollen records, the U-Net-based approach produces complete spatial coverage across Alaska and western Canada. This is achieved by training a U-Net model on the relationship between reconstructed land cover and environmental variables, and subsequently applying this learned mapping within the modern climatic space to infer land cover classes for all pixels in the study region. This step transforms sparse, record-centered reconstructions into spatially continuous paleo-landscapes, enabling the analysis of regional-scale patterns and trends that cannot be derived from the source-area data alone.

The reconstructed landscapes are dominated by a limited number of land cover classes. Across the study region, the most prominent classes are evergreen needle-leaved forest; sparse trees, shrubs and herbs; shrubland; and grassland. During the late Holocene, the relative frequencies of these major classes remain comparatively stable, indicating limited large-scale compositional change in the reconstructed land cover.

More pronounced shifts occur around 10 ka (see Fig. 4). From this point toward older time slices, evergreen needle-leaved forest cover declines progressively, with the reduction continuing toward 20 ka. This decrease is accompanied by an increase in sparse vegetation, which becomes more prominent around 10 ka but declines again toward 20 ka. Shrubland shows the opposite pattern: its relative cover decreases around 10 ka and increases again toward 20 ka. Overall, these temporal trends are broadly consistent with those observed in the Pixel Flow reconstructions.

In addition to these dominant trends, several less frequent classes become more apparent in the spatially continuous reconstruction. This includes flooded land cover classes, which occur more prominently in some time slices and regions than in the source-area product. These patterns should be interpreted cautiously, but they illustrate the ability of the U-Net-based approach to highlight spatially coherent land cover signals that may be difficult to detect from discontinuous source-area reconstructions alone.

The accuracy of the full model, validated against label data, decreases towards 10 ka and then increases again slightly (Fig. 5b). Across the study period, it ranges between 0̃.9 and 0̃.8. As expected, accuracy is lower where pollen records overlap because multiple observers (Fig. 3e)

3.3 Relative Uncertainty

The uncertainties associated with the two site-based reconstruction steps exhibit similar spatial patterns (Fig. 5a). Higher uncertainty is observed in the southeastern part of the study area, which coincides with regions characterized by extensive forest cover in the modern time slice. This pattern suggests that high forest cover increases the difficulty of both translating vegetation composition into land cover classes and distributing these classes across pixels within the pollen source area. Different forest types may be difficult to distinguish based on pollen-derived vegetation data alone, while the relatively narrow climatic space occupied by forested environments may lead to greater overlap among land cover classes in the RDA space. The remainder of the study area is characterized by low to intermediate relative uncertainty values. Slightly elevated uncertainties are also evident in central Alaska, another region dominated by forest cover.

Reconstruction performance was assessed using both absolute and weighted agreement metrics. Across all time slices, weighted agreement consistently exceeds absolute agreement, with a relatively stable offset of approximately 0.3 (Fig. 5b). For

https://doi.org/10.5194/egusphere-2026-4084
Preprint. Discussion started: 22 July 2026

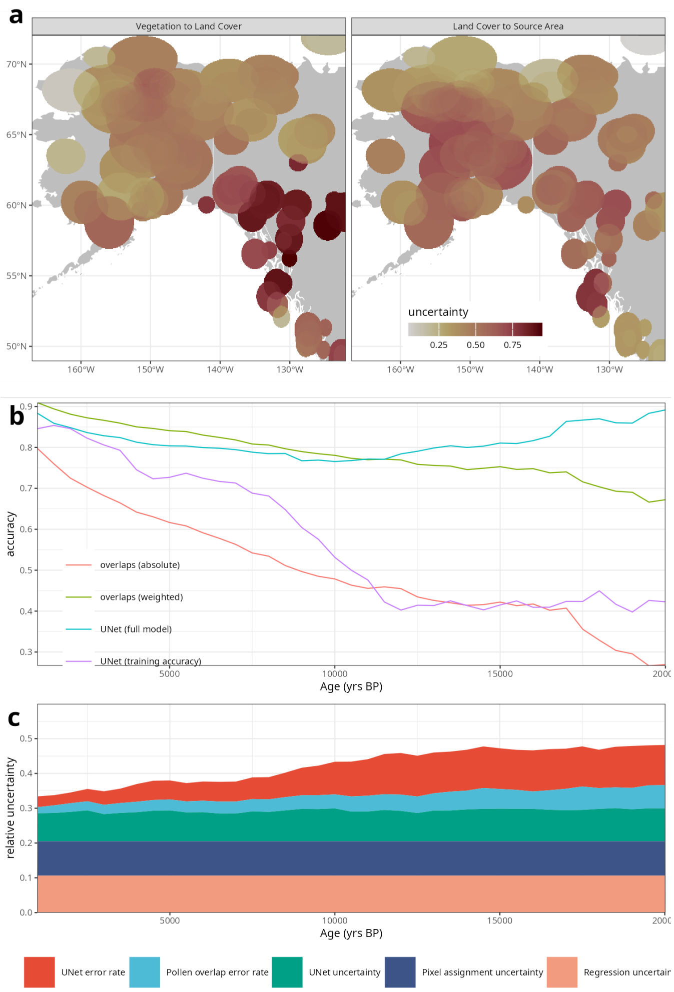

Figure 5. Relative uncertainty of pollen-based reconstruction for the source-area reconstruction (a), temporal agreement between reconstruction overlaps for absolute and weighted agreement, andabsolute accuracy of the full U-UNet model and training accuracy through time (b), and relative uncertainty for all pipeline steps combined

https://doi.org/10.5194/egusphere-2026-4084
Preprint. Discussion started: 22 July 2026

the most recent time slice, both agreement measures reach values close to 1. This reflects the use of ESA CCI land cover as input for this time slice. Minor deviations occur due to the transformation of anthropogenic land cover classes into potential natural vegetation based on their position in reduced-dimensional environmental space. A marked decline in agreement is observed between the modern reference and the first paleo time slice (1 ka BP). Beyond this point, agreement decreases progressively with increasing age. At 20ka BP, spatial averages of weighted and absolute agreement are approximately at 0.7 and 0.3, respectively.

The difference between weighted and absolute agreement remains relatively constant across time. In contrast, the absolute level of agreement decreases with increasing age.The number of overlapping pixels used for validation decreases for older time slices, resulting in increased variability in agreement estimates. Spatially, agreement values exhibit consistent patterns through time, with slightly higher agreement observed in central Alaska compared to surrounding regions. The U-Net's internal confidence decreases only slightly through time, but spatial patterns change (see Fig. 3d,5c). While confidence is homogeneous and intermediate in modern time slices, it becomes more heterogeneous through time, with areas of marked high confidence in northern tundra areas and along the southern coast, and lower confidence in central Alaska. U-Net training accuracy shows a clear temporal trend, decreasing with age and roughly following the same trend as the absolute agreement of pollen source area reconstructions (see Fig. 5b). Accuracy of the full U-Net model stays consistently high roughly ranging between 0.75 and 0.9 (see Fig. 5b). Total uncertainty is defined as the average of the uncertainties described above for each pixel and time slice. The spatial pattern is still largely dominated by uncertainty from the "Vegetation to Land Cover" and "Land Cover to Source Area" steps (see Fig. 3f). Fig. 5c illustrates the uncertainty contributions for each time slice. Overall uncertainty increases toward older time slices. "Vegetation to Land Cover" and "Land Cover to Source Area" are constant through time, whereas error rate of the pollen overlap and U-Net error rate increase and the U-Net uncertainty varies slightly through time. The highest total uncertainty is observed in the southeast of the study area, where pollen- record coverage is sparse.

3.4 Elevational Tree Cover Dynamics

To illustrate the analytical potential of the reconstruction, changes in the elevational distribution of evergreen needle-leaved forest were evaluated for an example site. This was quantified using the 90th percentile of elevation of all pixels classified as evergreen needle-leaved forest for each time slice, representing an approximation of the upper elevational limit of forest cover.

At the beginning of the record, forest cover is restricted to relatively low elevations, with the 90th percentile located at approximately 450 m (see Fig. . Over time, a general upward shift in elevation is observed. This trend culminates in an initial maximum around 10 ka BP, where the upper elevation reaches approximately 700 m. Following this peak, a moderate decline in elevation occurs before a second maximum is reached around 2.5 ka BP at nearly 750 m.

Three-dimensional renderings of the reconstructed landscapes provide additional context for these patterns, illustrating the spatial distribution of forest cover across both horizontal and vertical dimensions. In parallel to elevational changes, the proportional coverage of evergreen needle-leaved forest at this site also varies through time. Forest cover reaches its maximum extent of approximately 35% around 10 ka BP. Subsequently, it declines to roughly 15% by around 6 ka BP, followed by a gradual

https://doi.org/10.5194/egusphere-2026-4084
Preprint. Discussion started: 22 July 2026

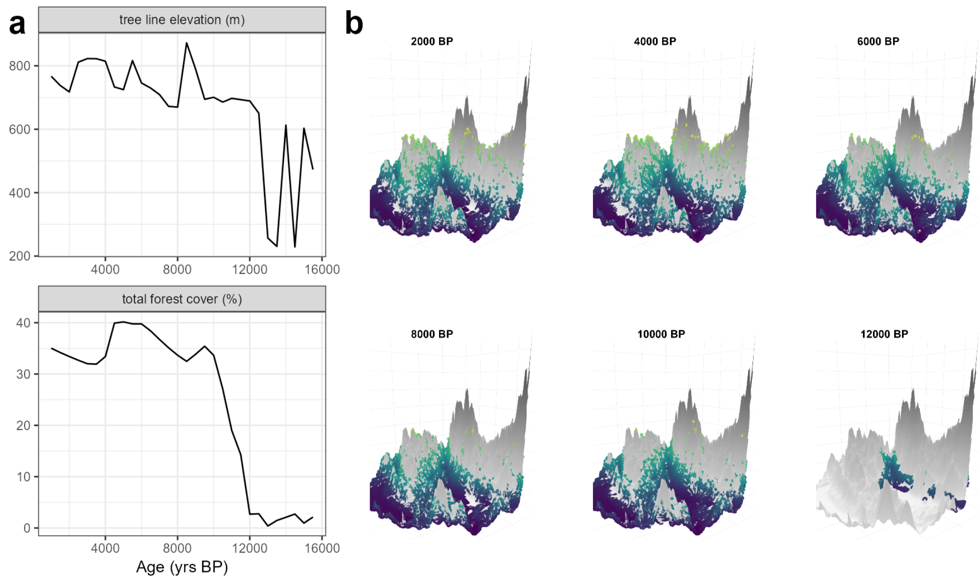

Figure 6. Treeline elevation application example. (a) Temporal trend of treeline elevation (90th percentile of evergreen needle-leaved forest pixel elevation) and of total forest cover within the example record's source area. (b) 3D rendering of evergreen needle-leaved forest pixels in space for six example time slices.

increase toward present-day values of approximately 20%. Together, these results highlight both vertical and areal dynamics of forest cover, demonstrating the capacity of the reconstruction to resolve spatiotemporal patterns in vegetation structure.

4 Discussion

4.1 Towards Spatially Explicit Paleo Land Cover

The presented pipeline enables the reconstruction of spatially explicit and temporally continuous paleo land cover based on pollen-derived vegetation data. It produces two complementary types of outputs: record-based reconstructions within pollen source areas and spatially continuous land cover maps generated through U-Net-based interpolation. In doing so, the approach transforms point-based paleoecological observations into gridded representations of past landscapes, allowing for spatially resolved analyses across large regions and extended time periods.

This development addresses a fundamental limitation of paleoecological data. Pollen records are typically sparse and site-based, which restricts their direct use for investigating spatial patterns and processes (Anderson et al., 2022). Many ecological and environmental questions, however, require continuous spatial information at finer resolutions. By providing land cover reconstructions at 300 m resolution across multiple time slices, the pipeline bridges the gap between localized proxy data and the spatially explicit datasets needed to study landscape-scale dynamics. This capability addresses a gap that remains only partially resolved by existing pollen-based reconstruction methods. Approaches such as REVEALS-GMRF (Pirzamanbein et al.,

https://doi.org/10.5194/egusphere-2026-4084
Preprint. Discussion started: 22 July 2026

2018, 2014) and the spatio-temporal random forest framework of Zhang et al. (2025) generate spatially continuous reconstructions across large regions, but typically operate on vegetation cover fractions at comparatively coarse spatial resolutions. In contrast, methods such as the Landscape Reconstruction Algorithm (Sugita, 2007a, b), the Extended Downscaling Approach (Theuerkauf and Couwenberg, 2017), and BACKLAND (Plancher et al., 2024) provide more detailed representations but remain closely linked to individual pollen records and their surrounding landscapes. The present framework seeks to bridge these approaches by combining regional spatial continuity with high-resolution land cover mapping, thereby extending pollen-based reconstructions toward representations that can be analyzed using concepts from landscape ecology. At the same time, the resulting reconstructions should not be interpreted as direct observations of past environments. Rather, the pipeline constitutes a reconstruction framework that produces data-constrained, model-based estimates of past land cover. These estimates are derived from the combination of pollen data, relationships between land cover and environmental conditions inferred from modern observations, and a set of methodological assumptions. The outputs therefore represent the most likely spatial distribution of land cover given the available information and constraints, rather than a definitive representation of past landscapes. A specific limitation of the current implementation is that dynamic glacial extent was not explicitly included as a temporal constraint. As a result, the model may assign vegetation classes to areas that were ice-covered during earlier time slices, particularly during the late glacial period. These cases represent ecologically implausible predictions rather than meaningful vegetation signals. Incorporating time-specific ice masks or dynamic non-vegetated constraints would therefore be an important improvement for future versions of the reconstruction framework.

An important aspect of the framework is the generation of two complementary reconstruction products. Source-area reconstructions retain a strong connection to the underlying pollen data and preserve local variability, reflecting conditions within the spatial influence of individual records. In contrast, the U-Net-based reconstructions provide a spatially continuous extension of the source-area product and impose spatial continuity across the entire study region, enabling the analysis of regional-scale patterns and trends. These two representations should be viewed as complementary perspectives, capturing different aspects of the same underlying system rather than providing competing interpretations.

The comparison of both products illustrates the practical consequences of this distinction. The U-Net-based reconstruction substantially increases spatial coverage because predictions are generated for all pixels across the study region, rather than only within pollen source areas. Consequently, the spatially continuous reconstruction contains a much larger number of reconstructed pixels; however, these additional pixels should be interpreted as model-based spatial interpolation rather than as additional paleoecological observations. Despite this difference in spatial coverage, the main temporal land cover trends are broadly consistent between the source-area and U-Net-based products. This suggests that the interpolation preserves the dominant vegetation signals contained in the pollen-based reconstructions while extending them into unsampled areas. Differences between the two products are nevertheless informative. The U-Net-based reconstruction shows more extensive tree cover in some regions and time slices, likely because large areas with high environmental suitability for forest are not represented by the available pollen source areas. In this sense, the spatially continuous reconstruction may partly compensate for spatial gaps in the pollen-record network, but it also depends on the assumption that relationships learned from sampled areas can be transferred to unsampled parts of the environmental space. Similarly, the smoother temporal development of some classes in the

https://doi.org/10.5194/egusphere-2026-4084
Preprint. Discussion started: 22 July 2026

pollen-based source-area data reflects the interpolation of vegetation composition within discrete time slices, whereas the U-Net output may introduce additional spatial smoothing through the model architecture and training settings. Future applications could therefore explore alternative U-Net configurations, loss functions, or ensemble approaches to better quantify the sensitivity of reconstructed class trends to model design. The distinction between these two reconstruction products also reflects a broader distinction among existing reconstruction methodologies. Source-area reconstructions remain closest to traditional pollen-based approaches by preserving a direct connection to the reconstructed vegetation signal. The spatially continuous reconstruction extends beyond this paradigm by inferring land cover distributions for unsampled locations and thereby emphasizing regional landscape structure. Rather than replacing record-based reconstructions, the continuous product complements them by enabling analyses that require complete spatial coverage, such as assessments of habitat connectivity, fragmentation, or large-scale landscape organization. The methodological novelty of the pipeline lies in the integration of multiple approaches. It combines multivariate regression techniques, projection into environmental space, and deep learning–based spatial interpolation within a unified framework. This allows for the generation of large-scale datasets comprising billions of spatially explicit pixels across long temporal sequences, which would not be achievable using traditional paleoecological methods alone.

A further distinction from previous reconstruction approaches is the focus on land cover rather than vegetation composition. Many established methods reconstruct taxonomic abundances, plant functional types, or biome affiliations, which provide important ecological information but are not directly comparable to modern land cover datasets. By generating land cover classes, the framework produces outputs that can be integrated more readily with remote sensing products (e.g. ESA, 2017), biodiversity analyses (e.g. Lu et al., 2024), and landscape ecological metrics (Kindlmann and Burel, 2008). This facilitates direct comparisons between past and present landscape structures and may help link paleoecological reconstructions to contemporary questions concerning habitat availability, connectivity, and ecosystem resilience under environmental change.

The validation results further indicate that prediction performance varies through both time and space. Accuracy declines toward 10 ka and increases again in older time slices. This pattern likely reflects a combination of reduced training support, changing environmental analogues, and increasing uncertainty in both the pollen-based reconstructions and environmental predictors further back in time. Spatially, higher accuracy in central Alaska suggests that predictions are most reliable in regions with stronger data support or better representation in the training domain, whereas peripheral and poorly sampled regions should be interpreted with greater caution.

As a result, the pipeline provides a foundation for investigating a wide range of paleoecological and paleoenvironmental questions. By enabling the analysis of spatial patterns, temporal dynamics, and landscape structure, it extends the scope of pollen-based reconstructions beyond site-level interpretations toward spatially explicit representations of past environments. More broadly, such reconstructions may help place contemporary ecological change into a longer-term context by allowing the investigation of how landscape structure and habitat distributions responded to past climatic transitions across millennial timescales.

https://doi.org/10.5194/egusphere-2026-4084
Preprint. Discussion started: 22 July 2026

4.2 Treeline elevation change and other use cases

The analysis of elevational treeline dynamics at the example site reveals a clear relationship between forest expansion and vertical distribution of vegetation. During the initial increase in evergreen needle-leaved forest cover during the early Holocene, a pronounced rise in the upper elevation limit of forested areas is observed. This suggests a rapid upslope expansion of tree cover following deglaciation and improving climatic conditions (Wieser et al., 2019).

Notably, although overall forest cover declines again after its early Holocene maximum, the upper elevational limit of forest does not decrease accordingly. This indicates that once higher elevations were colonized, they remained occupied and continued to provide suitable habitat for tree growth. In contrast, prior to this expansion, higher elevations were likely still influenced by glacial or periglacial conditions during the Late Glacial period and were dominated by more open land cover types such as tundra, shrubland, and other sparse vegetation. These conditions would have constrained forest distribution to lower elevations. The persistence of elevated treeline positions from 10 ka BP on, suggests that elevation, as a largely static environmental variable, provides a stable reference against which dynamic changes in land cover can be assessed. This example highlights how the reconstructed dataset enables the investigation of ecological dynamics at relatively fine spatial scales, capturing both horizontal and vertical changes in vegetation over time. Beyond this case study, the dataset supports a range of additional applications. For instance, analyses of wetland distribution could be used to quantify temporal changes in wetland extent and assess their implications for past carbon storage, thereby contributing to improved estimates of long-term carbon balances. Similarly, the spatially explicit nature of the reconstruction allows for the investigation of landscape connectivity and fragmentation, which is particularly relevant for understanding small-scale migration pathways of flora and fauna. By combining reconstructed land cover with fossil records or modern occurrence data, it becomes possible to explore how connectivity constraints may have influenced migration dynamics under past and ongoing climate change.

Further applications include the quantification of vegetation–climate feedbacks through changes in land cover composition, the reconstruction of past fire regimes by analyzing fuel availability and spatial continuity (potentially in combination with charcoal records), and the integration of land cover information into paleo-species distribution models to refine estimates of past habitat suitability. Together, these examples demonstrate that the presented reconstruction framework is not limited to descriptive mapping, but provides a flexible basis for a wide range of spatially explicit paleoecological analyses.

4.3 Sources of Uncertainty and Methodological Implications

Despite providing a robust and internally consistent reconstruction framework, the presented pipeline is subject to several sources of uncertainty that arise from both the underlying data and methodological assumptions. These uncertainties should be considered when interpreting the results. The uncertainty estimates presented here do not represent absolute reconstruction error, but rather relative indicators of where and when the reconstruction is less well constrained by the available data and model assumptions. The site-based uncertainty estimates indicate that uncertainty is not spatially uniform across the study region. Higher uncertainty in the southeastern part of the study area, and to a lesser extent in central Alaska, coincides with regions characterized by extensive forest cover. This pattern is likely related to the difficulty of separating structurally similar

https://doi.org/10.5194/egusphere-2026-4084
Preprint. Discussion started: 22 July 2026

forest classes using pollen-derived vegetation composition alone. Forested environments may occupy relatively narrow and overlapping regions of environmental space, making the translation from vegetation composition to discrete land cover classes less certain. In addition, once land cover classes are assigned, distributing these classes spatially within the pollen source area remains ambiguous where several forest classes are environmentally plausible. The higher uncertainty in forested regions therefore does not necessarily indicate unreliable reconstruction as a whole, but highlights areas where exact class assignment should be interpreted more cautiously.

A primary source of uncertainty is temporal in nature. The reconstruction proceeds sequentially backward in time, using modern land cover as a baseline and iteratively inferring prior states. As a consequence, errors introduced at each step may accumulate, leading to increasing uncertainty for older time slices. This is reflected in the declining agreement observed in the validation results. In addition, the temporal preprocessing of pollen data, specifically the binning and interpolation to regular 500-year intervals, introduces smoothing of the signal. While this improves comparability and usability, it may dampen short-term variability and obscure more abrupt vegetation changes.

The temporal decline in agreement further indicates that pixel-wise land cover assignment becomes progressively less constrained with age. The sharp decrease from the modern reference to the first paleo time slice reflects the transition from a reconstruction directly anchored in modern land cover data to fully model-derived paleo estimates. After this initial drop, the more gradual decline suggests cumulative uncertainty propagation through the sequential reconstruction. The consistently higher weighted agreement compared to absolute agreement indicates that many mismatches occur between similar land cover classes rather than between ecologically unrelated classes. Thus, even where exact class assignment differs, the reconstructions often retain broader structural similarity. This distinction is important, because it suggests that regional-scale trends and broad vegetation structure are more robust than individual pixel-level class identities.

The validation results should nevertheless be interpreted as a measure of internal consistency rather than external accuracy. No independent paleo land cover product exists at comparable spatial and temporal resolution, and the agreement metrics are derived from comparisons among reconstructions based on different pollen records. Although these reconstructions are generated separately, they are not fully independent because they share modern reference data, environmental predictors, and parts of the broader pollen-data structure. The agreement values therefore indicate how reproducibly the framework reconstructs land cover under partially independent data support, but they do not provide direct validation against true past land cover. The reduction in overlapping pixels toward older time slices additionally increases the variability of agreement estimates, making older validation results less stable.

Spatial uncertainties arise from the lack of explicit spatial constraints in the reconstruction procedure. Land cover class assignment is based solely on proximity in environmental space, without accounting for physical distance or dispersal limitations. This implies that land cover transitions can occur independently of realistic migration rates, which may be particularly problematic for vegetation types such as forests that expand over long timescales. As a result, reconstructed spatial patterns may exhibit unrealistic fragmentation or overly rapid shifts. This is similar to species distribution models without dispersal constraints (e.g. Holloway and Miller, 2017).

https://doi.org/10.5194/egusphere-2026-4084
Preprint. Discussion started: 22 July 2026

For the U-Net-based interpolation, additional uncertainties emerge in regions lacking direct pollen constraints. In these areas, land cover classes are inferred purely from learned relationships between environmental variables and reconstructed land cover, without direct observational support. This issue is exacerbated for older time slices, where fewer pollen records are available, reducing the amount of training data and increasing uncertainty in the interpolated outputs. The U-Net confidence estimates show that model confidence changes only moderately through time, but that its spatial structure becomes more heterogeneous. In modern time slices, confidence is relatively homogeneous and intermediate, whereas older time slices show areas of high confidence in northern tundra regions and along the southern coast, and lower confidence in parts of central Alaska. This suggests that the model becomes increasingly confident in environmentally distinct or more easily separable regions, while confidence declines in areas where class boundaries are more ambiguous or where several land cover classes occupy similar environmental space. Consequently, low-confidence areas in the U-Net product should be treated as regions where spatial interpolation is less certain, particularly when interpreting fine-scale class distributions.

Furthermore, as with many deep learning approaches, the U-Net model may still have a tendency to overrepresent dominant land cover classes, even though measures were taken to reduce this effect as much as possible (Japkowicz and Stephen, 2002; Megahed et al., 2021). This is particularly relevant for rare classes, including flooded land cover types, which may be sensitive to both class imbalance and local environmental predictors. Apparent spatial coherence in such classes should therefore be interpreted together with the uncertainty layers rather than as direct evidence of past landscape structure.

Several uncertainties are also data-driven. The reconstruction relies on the assumption that relationships between land cover classes and environmental conditions derived from modern data remain valid through time. This stationarity assumption is fundamental but may not fully hold under different paleoclimatic regimes (e.g. Juggins, 2013). In addition, unequal representation of land cover classes in the training data can introduce biases, as classes with lower occurrence are less well constrained. Anthropogenic land cover introduces an additional layer of complexity. Modern landscapes are heavily influenced by human activity, which can distort the inferred environmental space of land cover classes (e.g. Ellis, 2011). Although steps are taken to mitigate this effect by excluding or transforming anthropogenic classes, residual biases may persist and influence the reconstruction.

Another important limitation arises from the discretization of vegetation into a finite set of land cover classes. Continuous ecological gradients are thereby simplified into categorical representations, which may lead to misclassification, particularly between structurally similar classes (e.g. Foody, 1997; Levin, 1992). Consequently, some discrepancies in the reconstruction may reflect classification artifacts rather than true ecological differences.

A further consideration is the mismatch between the spatial resolution of the reconstruction and the effective source area of pollen data. While land cover is resolved at 300 m, pollen signals typically integrate vegetation over larger spatial extents. This scale discrepancy may lead to an overinterpretation of fine-scale spatial patterns that are not fully supported by the underlying data (Levin, 1992). In addition, the reconstruction represents one of potentially multiple plausible land cover configurations consistent with the input data. Due to the inherent ambiguity in translating pollen-derived signals into spatially explicit vegetation patterns, the solution is not unique. The pipeline therefore produces a deterministic estimate of the most likely land cover distribution given the imposed constraints, rather than an exhaustive, stochastic representation of all possible states, as has previously been implemented with Gaussian statistics (Pirzamanbein et al., 2018, 2014). The combined uncertainty estimate provides a practical way to identify regions and periods where reconstructed land cover should be interpreted with greater caution. Because total uncertainty is derived from multiple components, it reflects both site-based reconstruction uncertainty, temporal agreement uncertainty, and U-Net confidence. The resulting spatial pattern is strongly influenced by the uncertainty associated with the vegetation-to-land cover and land cover-to-source-area steps, which explains the consistently elevated values in the southeastern part of the study region. Temporal uncertainty increases toward older time slices, while U-Net uncertainty varies more subtly through time. The total uncertainty layer should therefore be used not as a binary mask separating valid and invalid reconstructions, but as contextual information for downstream analyses. For example, landscape metrics, class-area estimates, or habitat-connectivity analyses could be weighted by uncertainty, or repeated after excluding areas of high uncertainty to test the robustness of inferred patterns. The uncertainty estimation approach applied further limits the interpretation of reconstruction accuracy. As no independent paleo land cover data at comparable spatial resolution exist, estimation of uncertainty relies on regression performance, RDA metrics, comparisons between different overlapping reconstructions, and U-Net confidence. This provides a measure of internal consistency but does not constitute validation against an external ground truth. Potential avenues for future validation include the integration of independent proxy data such as ancient DNA, macrofossil records, or historical observations, although these would also require translation into comparable land cover classes.

Taken together, these aspects highlight important methodological implications. The pipeline favors consistency and reproducibility over ecological realism, producing smooth and spatially coherent land cover patterns that may underrepresent abrupt transitions or localized processes. As a result, the reconstructed landscapes should not be interpreted as exact representations of past environments, but rather as the most probable spatial distribution of land cover given the available data, assumptions, and constraints. Uncertainty increases with age, and interpretations of older time slices should therefore be made with particular caution. Spatially, areas with consistently high total uncertainty, particularly in the southeastern forested part of the study area and regions with sparse pollen-record coverage, should be interpreted less as precise local reconstructions and more as model-constrained estimates of broader land cover tendencies.

4.4 Improvements and Outlook

The presented pipeline constitutes a flexible framework for spatially explicit paleo land cover reconstruction, and several avenues exist to further improve its robustness, realism, and applicability. A key priority for future work is the incorporation of independent validation datasets. While current validation focuses on internal consistency, external constraints are required to better assess reconstruction accuracy. In this context, ancient DNA (aDNA) data represent a particularly promising source of localized vegetation information and should be explored in greater detail (Zimmermann et al., 2017). Additional proxy data, such as macrofossils or historical observations, may further contribute to multi-proxy validation approaches, although methodological challenges remain in translating these data into comparable land cover classes.

From a methodological perspective, the integration of spatial constraints represents a major opportunity for improvement. The current reconstruction operates in environmental space without accounting for physical distance, which may lead to un-

https://doi.org/10.5194/egusphere-2026-4084
Preprint. Discussion started: 22 July 2026

realistic spatial patterns for slowly migrating vegetation types. Future developments could incorporate dispersal limitations by estimating migration rates for different land cover classes based on modern observations and integrating these constraints into the pixel assignment procedure. This would allow for more realistic spatiotemporal dynamics, particularly for forest expansion processes.

Further refinements are also possible in the treatment of anthropogenic land cover. At present, anthropogenic classes are translated into potential natural vegetation, which may introduce inconsistencies across overlapping source areas. Developing a more generalized and spatially consistent approach to handling human-modified landscapes would improve the robustness of the reconstruction, particularly for more recent time periods.

An additional enhancement involves the integration of dynamic boundary conditions, such as changing ice cover. While paleoclimate reconstructions are often associated with substantial uncertainty, the extent of glaciation is comparatively well constrained. Incorporating time-varying ice masks from existing simulations would provide an important physical constraint on land cover distribution, preventing unrealistic class assignments in glaciated regions and improving overall spatial realism.

Beyond methodological improvements, the general framework is readily transferable to other regions and data sources. Expanding the spatial extent of the reconstruction to additional geographic areas would enable broader-scale analyses and facilitate interregional comparisons. Moreover, the pipeline is not inherently restricted to pollen data and could be adapted to alternative proxies capable of informing land cover, such as aDNA or other fossil-based datasets. This flexibility opens the possibility of multi-proxy reconstructions that combine complementary sources of paleoecological information. Finally, the reconstructed datasets provide a foundation for deriving additional environmental variables and for supporting downstream analyses. Future work may explore the integration of reconstructed land cover into models of carbon storage, fuel availability, or other ecosystem properties, further extending the utility of the approach. Continued application of the pipeline across diverse use cases will also be essential for assessing the realism and consistency of the generated reconstructions. Overall, these developments highlight the potential of the presented pipeline to evolve into a comprehensive framework for spatial paleoenvironmental reconstruction, supporting both methodological advancements and a wide range of scientific applications.

Code and data availability. R Code for the pollen-based land cover downscaling is available on Zenodo (Lisovski et al., 2026, https://doi.org/10.5281/zenodo.21219589). Python code to run the UNET on a spatial subset of the input data is available on Zenodo as well (Schild and Walsch, 2026, https://doi.org/10.5281/zenodo.21219614). Reconstructed vegetation data (Herzschuh et al., 2025, https://doi.org/10.1594/PANGAEA.974798), land cover data (ESA, 2017, https://doi.org/10.24381/cds.006f2c9a), topography (MacFerrin et al., 2025, http://dx.doi.org/10.7289/V5C8276M) and climate data (Brun et al., 2022, https://www.envidat.ch/#/metadata/bioclim_plus) are all available for download at the respective repositories. Final downscaled land cover for the study region can be found on Zenodo (Schild et al., 2026, https://doi.org/10.5281/zenodo.21240822).

https://doi.org/10.5194/egusphere-2026-4084
Preprint. Discussion started: 22 July 2026

Appendix A

Land Cover class overview. The column "merge to Class" indicates which land cover classes are to be combined together. The final land cover classes are, therefore, a bit coarser than the original classes in the CCI product (ESA, 2017). "Included in Class Calibration" states which classes were included in the RDA that creates the environmental land cover class density space (see Section 2.1.1). Anthropogenic classes are excluded at this point. "Predicted in Past" outlines which classes are included in the regression and can, thus, be predicted in the past. "Transfer" classes include those classes which are translated into potential natural vegetation for the first time step. Classes kept constant in the past are indicated in "Keep Constant in the Past" and classes that are set to zero in the past are listed under "Set to Zero in the Past".

Class Code	Class Name	Merge to Class	Include in Class Calibration	Predicted in Past	Transfer	Keep Constant in Past	Set to Zero in Past
0	No Data		FALSE	FALSE	FALSE	TRUE	FALSE
10	Cropland	15	FALSE	FALSE	TRUE	FALSE	TRUE
11	Cropland, Herbs	15	FALSE	FALSE	TRUE	FALSE	TRUE
12	Cropland, Trees or Shrubs	15	FALSE	FALSE	TRUE	FALSE	TRUE
15	Cropland		FALSE	FALSE	TRUE	FALSE	TRUE
20	Cropland, irrigated / post-flooding	15	FALSE	FALSE	TRUE	FALSE	TRUE
30	Major Mosaic Cropland, Minor Natural Veg.	15	FALSE	FALSE	TRUE	FALSE	TRUE
40	Major Natural Veg., Minor Mosaic Cropland	15	FALSE	FALSE	TRUE	FALSE	TRUE
50	Broadleaved, evergreen (>15%)		TRUE	TRUE	FALSE	FALSE	FALSE
60	Broadleaved, deciduous, closed to open	65	TRUE	TRUE	FALSE	FALSE	FALSE
61	Broadleaved, deciduous, closed	65	TRUE	TRUE	FALSE	FALSE	FALSE
62	Broadleaved, deciduous, open	65	TRUE	TRUE	FALSE	FALSE	FALSE
65	Broadleaved, deciduous (>15%)		TRUE	TRUE	FALSE	FALSE	FALSE
70	Needleleaved, evergreen, closed to open	75	TRUE	TRUE	FALSE	FALSE	FALSE
71	Needleleaved, evergreen, closed	75	TRUE	TRUE	FALSE	FALSE	FALSE
72	Needleleaved, evergreen, open	75	TRUE	TRUE	FALSE	FALSE	FALSE
75	Needleleaved, evergreen (>15%)		TRUE	TRUE	FALSE	FALSE	FALSE
80	Needleleaved, deciduous, closed to open	85	TRUE	TRUE	FALSE	FALSE	FALSE
81	Needleleaved, deciduous, closed	85	TRUE	TRUE	FALSE	FALSE	FALSE
82	Needleleaved, deciduous, open	85	TRUE	TRUE	FALSE	FALSE	FALSE
85	Needleleaved, deciduous (>15%)		TRUE	TRUE	FALSE	FALSE	FALSE
90	Mixed leaf type		TRUE	TRUE	FALSE	FALSE	FALSE
100	Major Mosaic Tree and Shrub, Minor Herbs	105	TRUE	TRUE	FALSE	FALSE	FALSE
110	Major Mosaic Herbs, Minor Tree and Shrub	105	TRUE	TRUE	FALSE	FALSE	FALSE
105	Mosaic Trees, Shrubs and Herbs		TRUE	TRUE	FALSE	FALSE	FALSE
120	Shrubland	125	TRUE	TRUE	FALSE	FALSE	FALSE
121	Evergreen Shrubland	125	TRUE	TRUE	FALSE	FALSE	FALSE
122	Deciduous Shrubland	125	TRUE	TRUE	FALSE	FALSE	FALSE
125	Shrubland		TRUE	TRUE	FALSE	FALSE	FALSE
130	Grassland		TRUE	TRUE	FALSE	FALSE	FALSE
140	Lichens and Mosses		FALSE	FALSE	FALSE	TRUE	FALSE
150	Sparse Tree, Shrub, Herbs	155	TRUE	TRUE	FALSE	FALSE	FALSE

https://doi.org/10.5194/egusphere-2026-4084
Preprint. Discussion started: 22 July 2026

Class Code	Class Name	Merge to Class	Include in Class Calibration	Predicted in Past	Transfer	Keep Constant in Past	Set to Zero in Past
151	Sparse Trees	155	TRUE	TRUE	FALSE	FALSE	FALSE
152	Sparse Shrubs	155	TRUE	TRUE	FALSE	FALSE	FALSE
153	Sparse Herbs	155	TRUE	TRUE	FALSE	FALSE	FALSE
155	Sparse Trees, Shrubs, Herbs (<15%)		TRUE	TRUE	FALSE	FALSE	FALSE
160	Trees, flooded, fresh	165	TRUE	TRUE	FALSE	FALSE	FALSE
170	Trees, flooded, saline	165	TRUE	TRUE	FALSE	FALSE	FALSE
165	Tree Cover, flooded		TRUE	TRUE	FALSE	FALSE	FALSE
180	Shrub or Herbaceous cover, flooded		TRUE	TRUE	FALSE	FALSE	FALSE
190	Urban Areas		FALSE	FALSE	TRUE	FALSE	TRUE
200	Bare Areas	205	FALSE	FALSE	FALSE	TRUE	FALSE
201	Consolidated Bare	205	FALSE	FALSE	FALSE	TRUE	FALSE
202	Unconsolidated Bare	205	FALSE	FALSE	FALSE	TRUE	FALSE
205	Bare Areas		FALSE	FALSE	FALSE	TRUE	FALSE
210	Water bodies		FALSE	FALSE	FALSE	TRUE	FALSE
220	Snow and Ice		FALSE	FALSE	FALSE	TRUE	FALSE
9999	No Data		FALSE	FALSE	FALSE	TRUE	FALSE

https://doi.org/10.5194/egusphere-2026-4084
Preprint. Discussion started: 22 July 2026

Appendix B

Table C1. Ecological distances between land cover classes derived from average RDA distances for all record locations in the study area (see Section 2.1.2).

	105	**125**	**130**	**155**	**165**	**180**	**65**	**75**	**85**	**90**	**50**	**15**	**140**	**190**	**205**	**210**	**220**
105	0.000	0.258	0.466	0.453	0.390	0.460	0.417	0.288	0.595	0.372	0.790	0.966	0.966	0.966	0.966	0.966	0.966
125	0.258	0.000	0.364	0.401	0.383	0.456	0.431	0.328	0.538	0.372	0.795	0.966	0.966	0.966	0.966	0.966	0.966
130	0.466	0.364	0.000	0.275	0.624	0.587	0.643	0.568	0.637	0.597	0.966	0.966	0.966	0.966	0.966	0.966	0.966
155	0.453	0.401	0.275	0.000	0.678	0.638	0.800	0.595	0.800	0.665	0.943	0.966	0.966	0.966	0.966	0.966	0.966
165	0.390	0.383	0.624	0.678	0.000	0.424	0.439	0.285	0.540	0.268	0.826	0.966	0.966	0.966	0.966	0.966	0.966
180	0.460	0.456	0.587	0.638	0.424	0.000	0.491	0.428	0.571	0.399	0.795	0.966	0.966	0.966	0.966	0.966	0.966
65	0.417	0.431	0.643	0.665	0.439	0.491	0.000	0.371	0.627	0.338	0.732	0.966	0.966	0.966	0.966	0.966	0.966
75	0.288	0.328	0.568	0.595	0.285	0.428	0.371	0.000	0.580	0.268	0.797	0.966	0.966	0.966	0.966	0.966	0.966
85	0.595	0.538	0.637	0.687	0.540	0.571	0.627	0.580	0.000	0.556	0.399	0.966	0.966	0.966	0.966	0.966	0.966
90	0.372	0.372	0.597	0.665	0.268	0.399	0.338	0.268	0.556	0.000	0.737	0.966	0.966	0.966	0.966	0.966	0.966
50	0.790	0.795	0.966	0.943	0.826	0.795	0.732	0.797	0.399	0.737	0.000	0.966	0.966	0.966	0.966	0.966	0.966
15	0.966	0.966	0.966	0.966	0.966	0.966	0.966	0.966	0.966	0.966	0.966	0.000	0.966	0.966	0.966	0.966	0.966
140	0.966	0.966	0.966	0.966	0.966	0.966	0.966	0.966	0.966	0.966	0.966	0.966	0.000	0.966	0.966	0.966	0.966
190	0.966	0.966	0.966	0.966	0.966	0.966	0.966	0.966	0.966	0.966	0.966	0.966	0.966	0.000	0.966	0.966	0.966
205	0.966	0.966	0.966	0.966	0.966	0.966	0.966	0.966	0.966	0.966	0.966	0.966	0.966	0.966	0.000	0.966	0.966
210	0.966	0.966	0.966	0.966	0.966	0.966	0.966	0.966	0.966	0.966	0.966	0.966	0.966	0.966	0.966	0.000	0.966
220	0.966	0.966	0.966	0.966	0.966	0.966	0.966	0.966	0.966	0.966	0.966	0.966	0.966	0.966	0.966	0.966	0.000

Author contributions. LS: investigation, methodology, software, validation, visualization, writing (original draft preparation), writing (review and editing); SL: methodology, software, investigation, visualization,writing (review and editing); PE: methodology, investigation, software, writing (review and editing); DC: methodology, writing (review and editing); JW: methodology, software, writing (review and editing); UH: conceptualization, investigation, methodology, funding acquisition, supervision, writing (review and editing)

Competing interests. The authors declare no competing interests.

Acknowledgements. This work was supported by Helmholtz Association's Initiative and Networking Fund through Helmholtz AI (grant no. ZT-I-PF-5-01), the Federal Ministry of Research, Technology and Space (grant no. BMFTR 03F0944A), and the PalMod Initiative (grant no. 01LP1510C). We also acknowledge technical support by Thomas Böhmer and the use of AI for language editing.

References

Aitchison, J.: The Statistical Analysis of Compositional Data, Journal of the Royal Statistical Society. Series B (Methodological), 44, 139–177, https://www.jstor.org/stable/2345821, 1982.

Anderson, L., Wahl, D. B., and Bhattacharya, T.: Understanding rates of change: A case study using fossil pollen records from California to assess the potential for and challenges to a regional data synthesis, Quaternary International, 621, 26–36, https://doi.org/10.1016/j.quaint.2020.04.044, 2022.

Badrinarayanan, V., Kendall, A., and Cipolla, R.: SegNet: A Deep Convolutional Encoder-Decoder Architecture for Image Segmentation, https://doi.org/10.48550/arXiv.1511.00561, arXiv:1511.00561 [cs.CV], 2016.

Bigelow, N. H., Brubaker, L. B., Edwards, M. E., Harrison, S. P., Prentice, I. C., Anderson, P. M., Andreev, A. A., Bartlein, P. J., Christensen, T. R., Cramer, W., Kaplan, J. O., Lozhkin, A. V., Matveyeva, N. V., Murray, D. F., McGuire, A. D., Razzhivin, V. Y., Ritchie, J. C., Smith, B., Walker, D. A., Gajewski, K., Wolf, V., Holmqvist, B. H., Igarashi, Y., Kremenetskii, K., Paus, A., Pisaric, M. F. J., and Volkova, V. S.: Climate change and Arctic ecosystems: 1. Vegetation changes north of 55°N between the last glacial maximum, mid-Holocene, and present, Journal of Geophysical Research: Atmospheres, 108, https://doi.org/10.1029/2002JD002558, _eprint: https://onlinelibrary.wiley.com/doi/pdf/10.1029/2002JD002558, 2003.

Blaauw, M. and Christen, J. A.: Flexible paleoclimate age-depth models using an autoregressive gamma process, Bayesian Analysis, 6, 457–474, https://doi.org/10.1214/11-BA618, 2011.

Bonneel, N., van de Panne, M., Paris, S., and Heidrich, W.: Displacement interpolation using Lagrangian mass transport, ACM Trans. Graph., 30, 1–12, https://doi.org/10.1145/2070781.2024192, 2011.

Bressan, P. O., Junior, J. M., Martins, J. A. C., Gonçalves, D. N., Freitas, D. M., Osco, L. P., Silva, J. d. A., Luo, Z., Li, J., Garcia, R. C., and Gonçalves, W. N.: Semantic Segmentation with Labeling Uncertainty and Class Imbalance, International Journal of Applied Earth Observation and Geoinformation, 108, 102 690, https://doi.org/10.1016/j.jag.2022.102690, arXiv:2102.04566 [cs.CV], 2022.

Brun, P., Zimmermann, N. E., Hari, C., Pellissier, L., and Karger, D. N.: CHELSA-BIOCLIM+ A novel set of global climate-related predictors at kilometre-resolution, https://doi.org/10.16904/ENVIDAT.332, artwork Size: 13194139533312 bytes, 423097 bytes Pages: 13194139533312 bytes, 423097 bytes, 2022.

Bunting, M. J., Gaillard, M.-J., Sugita, S., Middleton, R., and Broström, A.: Vegetation structure and pollen source area, The Holocene, 14, 651–660, https://doi.org/10.1191/0959683604hl744rp, 2004.

Davis, M. B.: On the theory of pollen analysis, American Journal of Science, 261, 897–912, https://doi.org/10.2475/ajs.261.10.897, 1963.

Ellis, E. C.: Anthropogenic transformation of the terrestrial biosphere, Philosophical Transactions of the Royal Society A: Mathematical, Physical and Engineering Sciences, 369, 1010–1035, https://doi.org/10.1098/rsta.2010.0331, 2011.

ESA: Land Cover CCI Product User Guide Version 2. [data set], https://doi.org/maps.elie.ucl.ac.be/CCI/viewer/download/ESACCI-LC-Ph2-PUGv2_2.0.pdf, 2017.

Faegri, K. and Iversen, J.: Text-book of modern pollen analysis, Geologiska Föreningen i Stockholm Förhandlingar, https://doi.org/10.1080/11035895009451859, 1950.

Fahrig, L.: Effects of Habitat Fragmentation on Biodiversity, Annual Review of Ecology, Evolution, and Systematics, 34, 487–515, https://doi.org/10.1146/annurev.ecolsys.34.011802.132419, 2003.

Foody, G. M.: Fully fuzzy supervised classification of land cover from remotely sensed imagery with an artificial neural network, Neural Computing & Applications, 5, 238–247, https://doi.org/10.1007/BF01424229, 1997.

https://doi.org/10.5194/egusphere-2026-4084
Preprint. Discussion started: 22 July 2026

Fordham, D. A., Jackson, S. T., Brown, S. C., Huntley, B., Brook, B. W., Dahl-Jensen, D., Gilbert, M. T. P., Otto-Bliesner, B. L., Svensson, A., Theodoridis, S., Wilmshurst, J. M., Buettel, J. C., Canteri, E., McDowell, M., Orlando, L., Pilowsky, J. A., Rahbek, C., and Nogues-Bravo, D.: Using paleo-archives to safeguard biodiversity under climate change, Science, 369, eabc5654, https://doi.org/10.1126/science.abc5654, 2020.

Franklin, J., Serra-Diaz, J. M., Syphard, A. D., and Regan, H. M.: Global change and terrestrial plant community dynamics, Proceedings of the National Academy of Sciences, 113, 3725–3734, https://doi.org/10.1073/pnas.1519911113, 2016.

Fulcher, B. D., Little, M. A., and Jones, N. S.: Highly comparative time-series analysis: the empirical structure of time series and their methods, Journal of The Royal Society Interface, 10, 20130 048, https://doi.org/10.1098/rsif.2013.0048, 2013.

Fyfe, R. M., de Beaulieu, J.-L., Binney, H., Bradshaw, R. H. W., Brewer, S., Le Flao, A., Finsinger, W., Gaillard, M.-J., Giesecke, T., Gil-Romera, G., Grimm, E. C., Huntley, B., Kunes, P., Kühl, N., Leydet, M., Lotter, A. F., Tarasov, P. E., and Tonkov, S.: The European Pollen Database: past efforts and current activities, Vegetation History and Archaeobotany, 18, 417–424, https://doi.org/10.1007/s00334-009-0215-9, 2009.

Githumbi, E., Fyfe, R., Gaillard, M.-J., Trondman, A.-K., Mazier, F., Nielsen, A.-B., Poska, A., Sugita, S., Theuerkauf, M., Woodbridge, J., Azuara, J., Feurdean, A., Grindean, R., Lebreton, V., Marquer, L., Nebout-Combourieu, N., Stancikaite, M., Tanţău, I., Tonkov, S., Shumilovskikh, L., and the LandClimII Data Contributors: European pollen-based REVEALS land-cover reconstructions for the Holocene: methodology, mapping and potentials, Earth System Science Data Discussions, pp. 1–61, https://doi.org/10.5194/essd-2021-269, 2021.

Haddad, N. M., Brudvig, L. A., Clobert, J., Davies, K. F., Gonzalez, A., Holt, R. D., Lovejoy, T. E., Sexton, J. O., Austin, M. P., Collins, C. D., Cook, W. M., Damschen, E. I., Ewers, R. M., Foster, B. L., Jenkins, C. N., King, A. J., Laurance, W. F., Levey, D. J., Margules, C. R., Melbourne, B. A., Nicholls, A. O., Orrock, J. L., Song, D.-X., and Townshend, J. R.: Habitat fragmentation and its lasting impact on Earth's ecosystems, Science Advances, 1, e1500 052, https://doi.org/10.1126/sciadv.1500052, 2015.

Herzschuh, U., Li, C., Böhmer, T., Postl, A. K., Heim, B., Andreev, A. A., Cao, X., Wieczorek, M., and Ni, J.: LegacyPollen 1.0: A taxonomically harmonized global Late Quaternary pollen dataset of 2831 records with standardized chronologies, Earth System Science Data Discussions, pp. 1–25, https://doi.org/10.5194/essd-2022-37, 2022.

Herzschuh, U., Böhmer, T., Li, C., Chevalier, M., Hébert, R., Dallmeyer, A., Cao, X., Bigelow, N. H., Nazarova, L., Novenko, E. Y., Park, J., Peyron, O., Rudaya, N. A., Schlütz, F., Shumilovskikh, L. S., Tarasov, P. E., Wang, Y., Wen, R., Xu, Q., and Zheng, Z.: LegacyClimate 1.0: a dataset of pollen-based climate reconstructions from 2594 Northern Hemisphere sites covering the last 30 kyr and beyond, Earth System Science Data, 15, 2235–2258, https://doi.org/10.5194/essd-15-2235-2023, 2023.

Herzschuh, U., Ewald, P., Schild, L., Li, C., and Böhmer, T.: LegacyVegetation: Northern Hemisphere reconstruction of past plant cover and total tree cover from pollen archives of the last 14 ka [data set], PANGAEA, p. 3 datasets, https://doi.org/10.1594/PANGAEA.974798, artwork Size: 3 datasets Medium: application/zip, 2025.

Holloway, P. and Miller, J. A.: A quantitative synthesis of the movement concepts used within species distribution modelling, Ecological Modelling, 356, 91–103, https://doi.org/10.1016/j.ecolmodel.2017.04.005, 2017.

IPBES: Global assessment report on biodiversity and ecosystem services of the Intergovernmental Science-Policy Platform on Biodiversity and Ecosystem Services, Tech. rep., Zenodo, https://doi.org/10.5281/ZENODO.3831673, version Number: 1, 2019.

IPCC: Climate Change 2023: Synthesis Report. Contribution of Working Groups I, II and III to the Sixth Assessment Report of the Intergovernmental Panel on Climate Change [Core Writing Team, H. Lee and J. Romero (eds.)]. IPCC, Geneva, Switzerland., Tech. rep., Intergovernmental Panel on Climate Change (IPCC), https://www.ipcc.ch/report/ar6/syr/, 2023.

Japkowicz, N. and Stephen, S.: The class imbalance problem: A systematic study1, Intelligent Data Analysis, 6, 429–449, https://doi.org/10.3233/IDA-2002-6504, 2002.

Joo, T., Chung, U., and Seo, M.-G.: Being Bayesian about Categorical Probability, https://doi.org/10.48550/arXiv.2002.07965, arXiv:2002.07965 [cs.LG], 2020.

Juggins, S.: Quantitative reconstructions in palaeolimnology: new paradigm or sick science?, Quaternary Science Reviews, 64, 20–32, https://doi.org/10.1016/j.quascirev.2012.12.014, 2013.

Kindlmann, P. and Burel, F.: Connectivity measures: a review, Landscape Ecology, 23, 879–890, https://doi.org/10.1007/s10980-008-9245-4, 2008.

Kramarczyk, P. and Hejmanowska, B.: UNET NEURAL NETWORK IN AGRICULTURAL LAND COVER CLASSIFICATION USING SENTINEL-2, The International Archives of the Photogrammetry, Remote Sensing and Spatial Information Sciences, XLVIII-1-W3-2023, 85–90, https://doi.org/10.5194/isprs-archives-XLVIII-1-W3-2023-85-2023, conference Name: 2nd GEOBENCH Workshop on Evaluation and BENCHmarking of Sensors, Systems and GEOspatial Data in Photogrammetry and Remote Sensing - 23–24 October 2023, Krakow, Poland, 2023.

Levin, S. A.: The Problem of Pattern and Scale in Ecology: The Robert H. MacArthur Award Lecture, Ecology, 73, 1943–1967, https://doi.org/10.2307/1941447, _eprint: https://esajournals.onlinelibrary.wiley.com/doi/pdf/10.2307/1941447, 1992.

Lin, T.-Y., Goyal, P., Girshick, R., He, K., and Dollár, P.: Focal Loss for Dense Object Detection, https://doi.org/10.48550/arXiv.1708.02002, arXiv:1708.02002 [cs.CV], 2018.

Lisovski, S., Ewald, P., Böhmer, T., and Schild, L.: PollenPixel: Source Area Reconstruction Code, https://doi.org/10.5281/zenodo.21219589, 2026.

Lu, X., Jia, Y., and Wang, Y.: The effect of landscape composition, complexity, and heterogeneity on bird richness: a systematic review and meta-analysis on a global scale, Landscape Ecology, 39, 132, https://doi.org/10.1007/s10980-024-01933-w, 2024.

MacFerrin, M., Amante, C., Carignan, K., Love, M., and Lim, E.: The Earth Topography 2022 (ETOPO 2022) global DEM dataset, Earth System Science Data, 17, 1835–1849, https://doi.org/10.5194/essd-17-1835-2025, 2025.

Mahmoud, A. S., Afify, N. M., Farg, E., Arafat, S. M., and Moustafa, M. S.: Enhancing land use and land cover mapping with uncertainty-aware 3D-UNet and Squeeze and Excite attention mechanism, International Journal of Image and Data Fusion, 17, 2613 386, https://doi.org/10.1080/19479832.2026.2613386, _eprint: https://doi.org/10.1080/19479832.2026.2613386, 2026.

Megahed, F. M., Chen, Y.-J., Megahed, A., Ong, Y., Altman, N., and Krzywinski, M.: The class imbalance problem, Nature Methods, 18, 1270–1272, https://doi.org/10.1038/s41592-021-01302-4, 2021.

Milletari, F., Navab, N., and Ahmadi, S.-A.: V-Net: Fully Convolutional Neural Networks for Volumetric Medical Image Segmentation, https://doi.org/10.48550/arXiv.1606.04797, arXiv:1606.04797 [cs.CV], 2016.

Nieto-Lugilde, D., Blois, J. L., Bonet-García, F. J., Giesecke, T., Gil-Romera, G., and Seddon, A.: Time to better integrate paleoecological research infrastructures with neoecology to improve understanding of biodiversity long-term dynamics and to inform future conservation, Environmental Research Letters, 16, 095 005, https://doi.org/10.1088/1748-9326/ac1b59, 2021.

Paszke, A., Chaurasia, A., Kim, S., and Culurciello, E.: ENet: A Deep Neural Network Architecture for Real-Time Semantic Segmentation, https://doi.org/10.48550/arXiv.1606.02147, arXiv:1606.02147 [cs.CV], 2016.

Pirzamanbein, B., Lindström, J., Poska, A., Sugita, S., Trondman, A.-K., Fyfe, R., Mazier, F., Nielsen, A. B., Kaplan, J. O., Bjune, A. E., Birks, H. J. B., Giesecke, T., Kangur, M., Latałowa, M., Marquer, L., Smith, B., and Gaillard, M.-J.: Creating spatially continuous

https://doi.org/10.5194/egusphere-2026-4084
Preprint. Discussion started: 22 July 2026

maps of past land cover from point estimates: A new statistical approach applied to pollen data, Ecological Complexity, 20, 127–141, https://doi.org/10.1016/j.ecocom.2014.09.005, 2014.

Pirzamanbein, B., Lindström, J., Poska, A., and Gaillard, M.-J.: Modelling Spatial Compositional Data: Reconstructions of past land cover and uncertainties, Spatial Statistics, 24, 14–31, https://doi.org/10.1016/j.spasta.2018.03.005, 2018.

Plancher, C., Mazier, F., Houet, T., and Gaucherel, C.: BACKLAND: spatially explicit and high-resolution pollen-based BACKward LAND-cover reconstructions, Ecography, 2024, e06 853, https://doi.org/10.1111/ecog.06853, _eprint: https://nsojournals.onlinelibrary.wiley.com/doi/pdf/10.1111/ecog.06853, 2024.

Prentice, C., Guiot, J., Huntley, B., Jolly, D., and Cheddadi, R.: Reconstructing biomes from palaeoecological data: a general method and its application to European pollen data at 0 and 6 ka, Climate Dynamics, 12, 185–194, https://doi.org/10.1007/BF00211617, 1996.

Ronneberger, O., Fischer, P., and Brox, T.: U-Net: Convolutional Networks for Biomedical Image Segmentation, https://doi.org/10.48550/ARXIV.1505.04597, version Number: 1, 2015.

Rull, V.: Palaeobiodiversity and taxonomic resolution: linking past trends with present patterns, Journal of Biogeography, 39, 1005–1006, https://doi.org/10.1111/j.1365-2699.2012.02735.x, _eprint: https://onlinelibrary.wiley.com/doi/pdf/10.1111/j.1365-2699.2012.02735.x, 2012.

Schild, L. and Walsch, J.: PollenPixel: U-Net, https://doi.org/10.5281/zenodo.21219614, 2026.

Schild, L., Ewald, P., Chenzhi, L., Hébert, R., Laepple, T., and Herzschuh, U.: LegacyVegetation: Northern Hemisphere reconstruction of past plant cover and total tree cover cover from pollen archives of the last 14 ka, Earth System Science Data, 2025.

Schild, L., Lisovski, S., Ewald, P., Walsch, J., Caus, D., and Herzschuh, U.: Output data for the Manuscript: From Pollen to Pixels: Spatial Downscaling of Holocene Land Cover Reconstructions, https://doi.org/10.5281/zenodo.21240823, 2026.

Schuhmacher, D., Bähre, B., Bonneel, N., Gottschlich, C., Hartmann, V., Heinemann, F., Schmitzer, B., and Schrieber, J.: transport: Computation of Optimal Transport Plans and Wasserstein Distances, https://cran.r-project.org/package=transport, 2024.

Seddon, A. W. R., Mackay, A. W., Baker, A. G., Birks, H. J. B., Breman, E., Buck, C. E., Ellis, E. C., Froyd, C. A., Gill, J. L., Gillson, L., Johnson, E. A., Jones, V. J., Juggins, S., Macias-Fauria, M., Mills, K., Morris, J. L., Nogués-Bravo, D., Punyasena, S. W., Roland, T. P., Tanentzap, A. J., Willis, K. J., Aberhan, M., van Asperen, E. N., Austin, W. E. N., Battarbee, R. W., Bhagwat, S., Belanger, C. L., Bennett, K. D., Birks, H. H., Bronk Ramsey, C., Brooks, S. J., de Bruyn, M., Butler, P. G., Chambers, F. M., Clarke, S. J., Davies, A. L., Dearing, J. A., Ezard, T. H. G., Feurdean, A., Flower, R. J., Gell, P., Hausmann, S., Hogan, E. J., Hopkins, M. J., Jeffers, E. S., Korhola, A. A., Marchant, R., Kiefer, T., Lamentowicz, M., Larocque-Tobler, I., López-Merino, L., Liow, L. H., McGowan, S., Miller, J. H., Montoya, E., Morton, O., Nogué, S., Onoufriou, C., Boush, L. P., Rodriguez-Sanchez, F., Rose, N. L., Sayer, C. D., Shaw, H. E., Payne, R., Simpson, G., Sohar, K., Whitehouse, N. J., Williams, J. W., and Witkowski, A.: Looking forward through the past: identification of 50 priority research questions in palaeoecology, Journal of Ecology, 102, 256–267, https://doi.org/10.1111/1365-2745.12195, _eprint: https://onlinelibrary.wiley.com/doi/pdf/10.1111/1365-2745.12195, 2014.

Shrivastava, A., Gupta, A., and Girshick, R.: Training Region-based Object Detectors with Online Hard Example Mining, https://doi.org/10.48550/arXiv.1604.03540, arXiv:1604.03540 [cs.CV], 2016.

Sudre, C. H., Li, W., Vercauteren, T., Ourselin, S., and Jorge Cardoso, M.: Generalised Dice Overlap as a Deep Learning Loss Function for Highly Unbalanced Segmentations, Deep learning in medical image analysis and multimodal learning for clinical decision support: Third International Workshop, DLMIA 2017, and 7th International Workshop, ML-CDS 2017, held in conjunction with MICCAI 2017 Quebec City, QC,..., 2017, 240–248, https://doi.org/10.1007/978-3-319-67558-9_28, 2017.

https://doi.org/10.5194/egusphere-2026-4084
Preprint. Discussion started: 22 July 2026

Sugita, S.: Theory of quantitative reconstruction of vegetation I: pollen from large sites REVEALS regional vegetation composition, The Holocene, 17, 229–241, https://doi.org/10.1177/0959683607075837, 2007a.

Sugita, S.: Theory of quantitative reconstruction of vegetation II: all you need is LOVE, The Holocene, 17, 243–257, https://doi.org/10.1177/0959683607075838, 2007b.

Theuerkauf, M. and Couwenberg, J.: The extended downscaling approach: A new R-tool for pollen-based reconstruction of vegetation patterns, The Holocene, 27, 1252–1258, https://doi.org/10.1177/0959683616683256, 2017.

Tian, F., Cao, X., Dallmeyer, A., Lohmann, G., Zhang, X., Ni, J., Andreev, A., Anderson, P. M., Lozhkin, A. V., Bezrukova, E., Rudaya, N., Xu, Q., and Herzschuh, U.: Biome changes and their inferred climatic drivers in northern and eastern continental Asia at selected times since 40 cal ka bp, Vegetation History and Archaeobotany, 27, 365–379, https://doi.org/10.1007/s00334-017-0653-8, 2018.

Venables, W. N. and Ripley, B. D.: Modern applied statistics with S, Statistics and computing, Springer, New York, 4th ed edn., ISBN 978-0-387-95457-8, 2002.

Vincens, A., Lézine, A.-M., Buchet, G., Lewden, D., and Le Thomas, A.: African pollen database inventory of tree and shrub pollen types, Review of Palaeobotany and Palynology, 145, 135–141, https://doi.org/10.1016/j.revpalbo.2006.09.004, 2007.

Wieser, G., Oberhuber, W., and Gruber, A.: Effects of Climate Change at Treeline: Lessons from Space-for-Time Studies, Manipulative Experiments, and Long-Term Observational Records in the Central Austrian Alps, Forests, 10, 508, https://doi.org/10.3390/f10060508, 2019.

Williams, J. W., Shuman, B. N., Webb III, T., Bartlein, P. J., and Leduc, P. L.: Late-Quaternary Vegetation Dynamics in North America: Scaling from Taxa to Biomes, Ecological Monographs, 74, 309–334, https://doi.org/10.1890/02-4045, _eprint: https://onlinelibrary.wiley.com/doi/pdf/10.1890/02-4045, 2004.

Williams, J. W., Grimm, E. C., Blois, J. L., Charles, D. F., Davis, E. B., Goring, S. J., Graham, R. W., Smith, A. J., Anderson, M., Arroyo-Cabrales, J., Ashworth, A. C., Betancourt, J. L., Bills, B. W., Booth, R. K., Buckland, P. I., Curry, B. B., Giesecke, T., Jackson, S. T., Latorre, C., Nichols, J., Purdum, T., Roth, R. E., Stryker, M., and Takahara, H.: The Neotoma Paleoecology Database, a multiproxy, international, community-curated data resource, Quaternary Research, 89, 156–177, https://doi.org/10.1017/qua.2017.105, 2018.

Zeller, K. A., Lewison, R., Fletcher, R. J., Tulbure, M. G., and Jennings, M. K.: Understanding the Importance of Dynamic Landscape Connectivity, Land, 9, 303, https://doi.org/10.3390/land9090303, 2020.

Zhang, P., Luo, Y., Liu, D., Wang, X., and Wang, T.: Pollen-based reconstruction of spatially-explicit vegetation cover over the Tibetan Plateau since the last deglaciation, Earth System Science Data, 17, 5557–5570, https://doi.org/10.5194/essd-17-5557-2025, 2025.

Zimmermann, H. H., Raschke, E., Epp, L. S., Stoof-Leichsenring, K. R., Schirrmeister, L., Schwamborn, G., and Herzschuh, U.: The history of tree and shrub taxa on bol'shoy lyakhovsky Island (New Siberian Archipelago) since the last interglacial uncovered by sedimentary ancient DNA and pollen data, Genes, 8, https://doi.org/10.3390/genes8100273, 2017.

Zou, H. and Hastie, T.: Regularization and Variable Selection Via the Elastic Net, Journal of the Royal Statistical Society Series B: Statistical Methodology, 67, 301–320, https://doi.org/10.1111/j.1467-9868.2005.00503.x, 2005.